Technische Universität Berlin
Fakultät II – Mathematik und Naturwissenschaften

Bachelorarbeit

Signal selection optimization for the Vector Fusion Category in the WZ $\rightarrow \ell\nu\ell\ell$ resonance search analysis performed in ATLAS at the LHC

Dennis Kraft
Physik B. Sc.
Matrikel-Nr. 375136

Berlin, 6. Juli 2021

Betreuer: Prof. Dr. Michael Lehmann
Prof. Dr. Michael Kobel

Zusammenfassung

Das Standardmodell der Teilchenphysik ist derzeit das beste Modell, um die Eigenschaften von Elementarteilchen und deren Wechselwirkung miteinander zu beschreiben. Auch wenn es durch viele Experimente immer wieder bestätigt wurde, gibt es bekannte physikalische Phänomene, die mit dem Standardmodell nicht erklärt werden können und eine Erweiterung der Theorie erfordern. Bestimmte neue Physikmodelle mit erweiterten Higgs-Sektoren können Antworten auf einige seit langem bestehende Fragen der Teilchenphysik liefern, wie zum Beispiel den Ursprung der Neutrinomasse, die Identität der Dunklen Materie und die Realisierung eines starken Phasenübergangs erster Ordnung für die elektroschwache Baryogenese. Das Georgi-Machacek Modell entspricht einem solchen Benchmark-Modell, das ein neues Resonanz-Higgsteilchen vorhersagt. In dieser Arbeit werden die Phasenräume verschiedener Variablen für einen ausschließlich leptonischen Zerfallskanal so optimiert, dass anhand der Signifikanz Auswahlkriterien gewählt werden. Diese werden dann durch die Berechnung der figures of merit validiert. Die bereits in der Resonanzanalyse verwendete Auswahl wird zunächst optimiert, indem der Cut Wert für bestimmte Variablen modifiziert wird. Diese werden gegebenenfalls angepasst und mit den alten Werten verglichen. Weiterhin werden einige neue Diskriminanzvariablen daraufhin untersucht, ob eine gleich gute Trennung zwischen Hintergrund- und Signalbereichen möglich ist. Schließlich wird eine neue Signifikanz Definition verwendet. Hier wird es interessant, ob sich die Auswahlkriterien ändern oder ob sich eine Änderung der figures of merit bemerkbar macht. Die Optimierung erfolgt für den betrachteten Resonanzprozess, kann aber aufgrund des ähnlichen Verhaltens der Zerfallsprodukte auch auf den Standardmodell Prozess der Vektorbosonenstreuung übertragen werden.

Abstract

The Standard Model of particle physics is currently the best model to describe the properties of elementary particles and their interaction with each other. Even if it has been confirmed by many experiments over and over, there are known physics phenomena that cannot be explained by the Standard Model and require an extension of the theory. Certain new physics models, with extended Higgs sectors may hold answers to some long-lasting questions in particle physics, such as the origin of neutrino mass, the identity of dark matter, and the realization of a strong first-order phase transition for electroweak baryogenesis. The Georgi-Machacek model corresponds to such a benchmark model, which predicts a new resonance Higgs particle. In this work, the phase spaces of different variables are optimized for an exclusively leptonic decay channel in such a way that selection criteria are chosen with the aid of the significance. These are then validated by calculating the figures of merit. The selection that are already used in the resonance analysis is first optimized by modifying the cut value for certain variables. If necessary, these will be adjusted and compared with the old values. Furthermore, some new discriminant variables are examined to see whether there is an equally good separation between background and signal regions possible. Finally, a new significance definition is used. Here it gets interesting whether the selection criteria are changing or whether this changes the figures of merit noticeable. The optimization takes place for the considered resonance process, but due to the similar behavior of the decay products, it can also be transferred to the Standard Model process of vector boson scattering.

Inhaltsverzeichnis

1. Introduction

The Standard Model (SM) of particle physics has been one of the main achievements of the last decades. It helps us understand the behavior and properties of all known elementary particles. Not only the confirmed predictions by a lot of experiments, but it's also used as an elegant theory to combine the fundamental forces, except gravitation.
The Large Hadron Collider (LHC) has very much contributed to complete our understanding of the SM. So it was the ATLAS and CMS experiment, who were able to discover in 2012 the long ago predicted Higgs particle. Its existence is important to physicists since it preserves unitary and explains the theory of spontaneous symmetry breaking.
The ATLAS detector has been a tool to verify the SM and for research beyond the current theory, which shall explain the open questions in particle physics, like the unification of SM and the gravitation of general relativity or the energy-matter dispersion in our universe. The Georgi-Machacek (GM) model is one of the benchmark models we look at the LHC. It predicts a charged Higgs particle with extended Higgs sector produced by quark-antiquark fusion or vector boson fusion.
For the thesis a fully leptonic channel will be considered ($\ell\nu\ell\ell$). The reason is the small amount of background compared to the hadronic decay channel and the accurate measurements of the leptons compared to the jets in the ATLAS detector. The low signal cross-section due to the small branching decay fraction will be compensated by the huge collision numbers produced at LHC.
This study will investigate vector boson scattering (VBS), which is a prediction by the SM. It allows the interaction between the weak gauge bosons with a triple or quartic coupling structure. These processes show similar behavior as the considered GM process. Because these couplings can be mediated by a Higgs boson, the analysis is sensitive to the SM VBS and also to the Higgs mechanism.
For a good evaluation of the data detected during the runs at the ATLAS experiment, it's helpful to reject as much background as possible. Also one pursues to find phase spaces with a high signal contribution. So in the end, one can decide whether the experimental data confirm a certain theory. By looking at the ratio between signal and background and cutting away certain areas one can optimize these phase spaces. Precisely calculating the significance of the different bins and finding the optimal range. This is done using discriminant variables like angles and momenta measured by the detector. Afterward, the cuts can be validated by specific figures of merit.
The investigation includes the optimization of cut values, which are used in current resonance analysis. Additionally, it investigates the potential of new variables, which were not considered before but might have a good discrimination power between background and signal contribution. Since the GM model predicts the resonance particle but not its mass, one needs to look at different mass points. As performing the optimization for each mass is expensive, the study shall consider possible masses between 225 and 1000 GeV as reference points for

low and high mass kinematic behavior.
In the end, a different significance definition is tested, to see its effect on the optimized phase spaces and the validation.

2. Theory

2.1. Standard Model

The ambition of particle physicists is to describe the elementary particles which are the constituents of the known matter of our universe and the fundamental interactions between them. For that reason, a theory has been formulated in the 70s to get a unified picture. In physics, all so far known forces between matter can be described by strong, weak, electromagnetic, and gravitational interaction. Except for the gravitation, all these are included in the theory of the Standard Model (SM), hence the gravitational couplings at the particle dimension are relatively weak. Since these particles are relatively small and they can move close to the speed of light, this quantum field theory (QFT) combines aspects from quantum mechanics and relativistic theory. Because this is not a theoretical work, the section shall only give the basic ideas of the particles and the possible interactions predicted by SM. For a deeper view into theory and its calculation one can refer to [1] .

2.1.1. Gauge bosons

By the new interpretation of interaction by Quantum field theory, the coupling between two fermions is described by the exchange of mediating particles. These have integer spin and are therefore called bosons. Because the description of the fundamental interactions is derived by the requirement of local gauge theory these are also known as gauge bosons. The interactions by electromagnetism, described in Quantum Electrodynamics (QED), and the weak force is unified elegantly by the electroweak theory with the photon and W, Z bosons as associated mediators. The theory of the strong interaction is the Quantum Chromodynamics (QCD) with eight associated gluons as exchange particles. The different force carriers and their properties are listed in 2.1. One can see that they are all massless except for the $W^{\pm}$ and Z boson.
During the development of the SM, there was one major problem that occurred, that in theory matter and mediator particles should be massless, however, it's experimentally proved that they are not, like fermions or the massive W, Z-Bosons. To solve this violation, theorists have developed the concept of spontaneous symmetry breaking. This proposes a new Higgs-field that is omnipresent and ensures the masses of the other particles by interacting with them. Besides this implies the existence of an associated particle the Higgs boson.

2.1.2. Matter particles

The basic framework our matter is made of is the atom. This consist furthermore of electrons, which are elementary particles, moving around the nucleus. The protons and neutrons in the nucleus additionally have a substructure of quarks. Together with the neutrinos, they are till now the common elementary particles. These particles have half-integer spin and are

Force	Strength	Boson		Spin	mass/GeV
Strong	1	Gluon	g	1	0
Electromagnetism	10^{-3}	Photon	γ	1	0
Weak	10^{-8}	$W^{\pm}$ boson	W	1	80.4
		Z boson	Z	1	91.2
Gravity	10^{-37}	Graviton?	G	2	0

Tab. 2.1.: Mediators/Bosons with their associated interactions, spin and mass given by [1]

	Leptons			Quarks		
	Particle	Q	mass/GeV	Particle	Q	mass/GeV
First generation	electron e	-1	0.0005	down (d)	-1/3	0.003
	neutrino ν_e	0	10^{-9}	up (u)	+2/3	0.005
Second generation	muon μ	-1	0.106	strange (s)	-1/3	0.1
	neutrino ν_μ	0	10^{-9}	charm (c)	+2/3	1.3
Third generation	tau τ	-1	1.78	bottom	-1/3	4.5
	neutrino ν_τ	0	10^{-9}	top (t)	+2/3	174

Tab. 2.2.: Elementary particles/Fermions of the SM with their electric charge and mass given by [1]

therefore called fermions. These can be subdivided into quarks and leptons. The quarks are the only fermions carrying color charge and therefore interact via the strong force. There are two types of quarks considering the electric charge q, with the up-type $q = \frac{2}{3}e$ and down-type $q = -\frac{1}{3}e$. They all occur in three different color charges. They are not observed individually but confined in so-called hadrons as colorless states. Leptons do not interact by the strong force. These include electrons and neutrinos. The electrically neutral neutrinos do not feel the electromagnetic force. All fermions participate in the weak interaction. For each of the four known fermions there are two copies with the same properties, but higher masses. They are called second and third generations of the associated particle. Their mass and electric charge are presented in 2.2. For each of the matter particles exist an anti-particle with the same mass but opposite charge.

2.1.3. Vector boson scattering

The thesis investigates a certain interaction between W and Z boson. Therefore it's important to know which couplings are predicted by the SM and what might be possible for higher energy scales when considering models beyond the SM. Since the W and Z Bosons carry the weak charge in the SM, the interaction between them is unlike for the photon, possible. This kind of coupling has been studied for QCD as well, but here it becomes more interesting considering the connection to the EWK symmetry breaking and the stronger coupling of the W and Z to the Higgs Boson. This work aims to optimize phase spaces for a special resonance labeled in the framework of the vector boson scattering (VBS) process. The term VBS describes all possible couplings with two EWK bosons at initial and final state in the form: VV $\longrightarrow$ VV. Interaction between EWK bosons predicted by SM includes triple and quartic gauge couplings. Additionally, diagrams can occur where the scattering is mediated by exchanging Higgs-Boson.

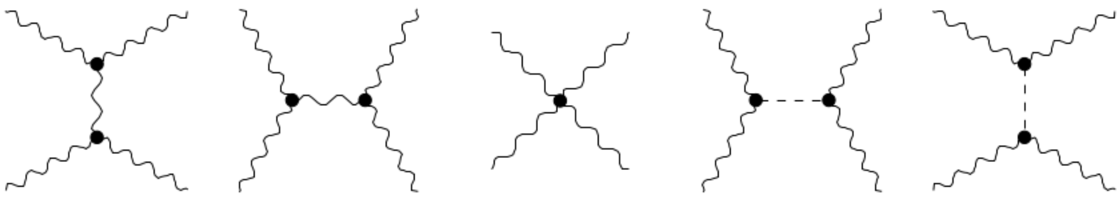

Abb. 2.1.: Feynman diagrams for SM predicitons with two initial and two final state gauge bosons in $VV \to VV$, wiggly line represents electroweak boson, dashed line represents the Higgs boson [2]

Considering leading order there are several Feynman diagrams possible contributing to VBS process 2.1. The huge masses of the scattering bosons make the coupling in the EWK sector of particular interest, due to the strong coupling to the Higgs boson.

2.1.4. Background process

In particle physics, while trying to measure a certain signal, there are always disruptive events labeled as background. The detector can not distinguish between them and the signal, since these are produced by processes with the same final state (here $\ell\nu\ell\ell$). So they are a major part of the measured data. There are different kind of backgrounds, depending on which interactions take part. Some of them occur by misidentification of the final state particles. Because there is an endless number of such processes they are merged into different labels.
Starting with the largest contribution, the WZ QCD features all processes with at least one strong interaction. Secondly, the WZ EWK background, which describes all processes with electroweak interaction only. This includes the VBS process from section 2.1.3 as well. The difference in proportion between these two is due to the larger coupling constant of the strong interaction compared to the electroweak $\alpha_s > \alpha_{EW}$ [1]. Other backgrounds are labeled appropriate to the participating particles in VV, V+jets, Top, and ttV, with V as a shortcut for a heavy vector boson. The remaining processes are merged into the other prompt label. Some examples are illustrated in Appendix D.

2.2. Beyond Standard Model - GM model

Although current experiments are described with great precision, the SM still leaves some open questions. The current research is working on developments and extensions of the theory to answer these or with the purpose of unification of different theories. Here the considered Georgi-Machacek model predicts a resonance provoked by quark-antiquark (qqf) or vector boson fusion (VBF) into a Higgs-fiveplet particle. The optimization will be performed for a process shown in the Feynman diagram in 2.2, including the decay of the $H_5^{\pm}$ into W and Z bosons. In the study, a fully leptonic channel is considered, so the bosons decay into three leptons (e, μ) and one neutrino. Because the model only predicts the existence of the particle but not its mass, the optimization needs to be sensitive to a wide range of possible masspoints, between 225 and 1000 GeV.

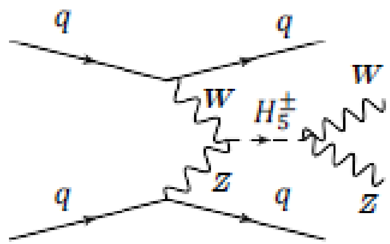

Abb. 2.2.: Feynman diagram for the considered signal process of vector boson fusion predicted by the GM model [3]

2.3. Experiment

2.3.1. Large Hadron Collider

Considering collision energy and luminosity the Large Hadron Collider is the most powerful particle accelerator in the world, build to discover new physics in high energy scales. With the shape of a ring of 26,6 km circumferences, divided into 8 sections, one of them hosting the Atlas experiment. Other participating experiments cover different purposes. The protons were accelerated up to 7 TeV each in opposite directions and collide at the interaction point at the center of the detector. This leads to a center-of-mass energy of $\sqrt{s} = 14TeV$, which is the energy available to unbound the quarks in the protons and produce high energetic particles. Another advantage the construction has compared to other colliders is the huge number of collisions that can be produced. This quantity is measured by the luminosity L. The number of events per time can be calculated via:

$$\frac{dN}{dt} = \sigma L \tag{2.1}$$

where σ is the cross-section, which indicates how likely it is for a specific process to occur. The luminosity L depends further on the number of particles per bunch, the number of bunches per beam, and the revolution frequency. To measure a certain process with low σ its important to increase L by changing the experiment setup on increases the total number of events other a certain time. By doing this one may reduce the statistic uncertainty. In this work the evaluated distributions will show the number of events over the discriminant variable, therefore often the time-integrated-luminosity will be given in fb^{-1}.

2.3.2. Atlas Experiment

The ATLAS detector is beside the CMS detector responsible for the discovery of the Higgs Boson in 2012. It can be subdivided into 3 different parts, cylindrical disposed around the beam axis. The detailed display is shown in 2.3. The following described from inner to outer layers. Its structure is chosen to fulfill some general purposes like good angular coverage, momentum resolution, precise energy measurement, identification, and trajectory reconstruction of different decay products after the collision. The subcomponents are arranged around the beam pipe described in the following from the inner to the outer parts of the detector.

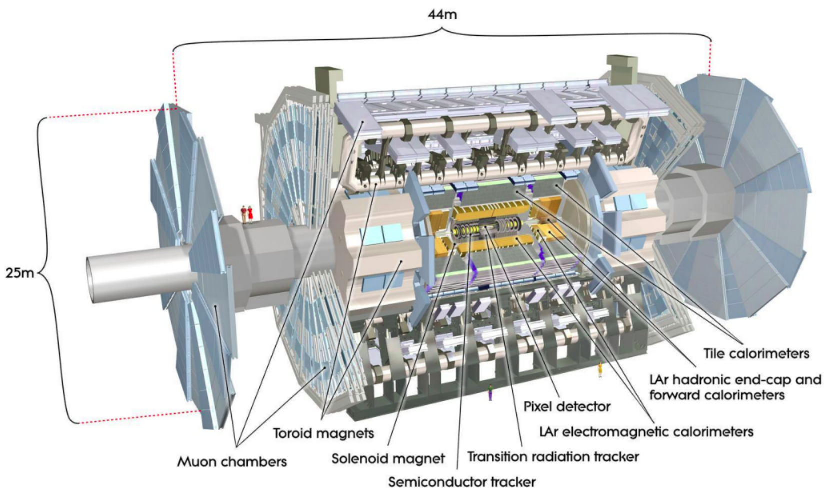

Abb. 2.3.: ATLAS detector with the individual partitions [4]

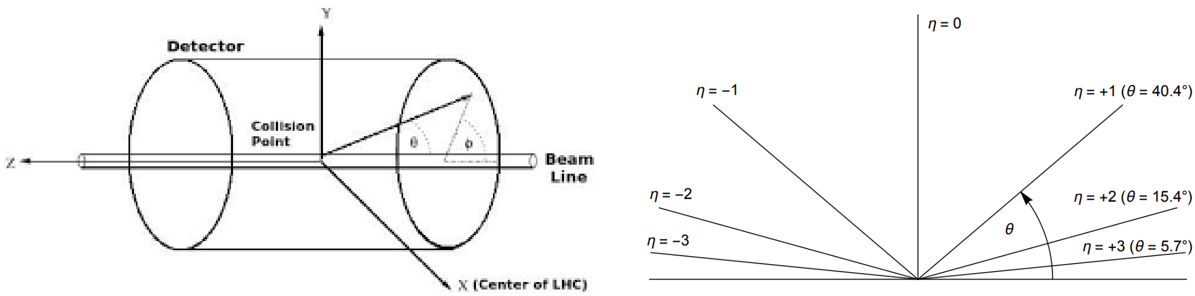

Abb. 2.4.: Left - commonly used coordinate system in ATLAS, with Collision Point in the center [5]
Right - Values of pseudorapidity illustrated for different angles of Θ [6]

Beginning with the high-resolution inner detector which is important for track reconstruction of the early decreasing particles like electrons or hadrons. Behind that, there are the different kind of calorimeters, designed for precise energy measurement. The only particles capable of escaping these layers are the muons and neutrinos. Therefore the outermost part of the muon chamber can easily identify a muon and due to the size of this component, can also determine precisely their momentum and energy. The detector is located in a magnetic field. Thus the transverse momentum of charged particles bend by the field can be calculated by the radius of the curvature.
Since the passing neutrinos are not measurable for the detector there is only an indirect way. In the process, the two protons colliding there is an unknown amount of momentum along the z-axis. Therefore in the transverse plane, the momentum p_T of all outgoing particles and their decay products must be 0. This can be used since all other particles p_T can be calculated and the missing transverse energy determined, with the neutrinos considered massless.

2.3.3. Coordinate system and variables

The commonly used notation in ATLAS is important to understand the different variables and phase spaces in the distributions and why they were selected for the optimization. The associated coordinate system is shown in 2.4 left. It's right-handed with z parallel to the beam axis. Often the azimuthal and polar angles Θ and Φ will be used instead. To describe the particles boost along the z-axis, the pseudo-rapidity η is introduced as:

$$\eta = -\ln(\frac{\Theta}{2}) \tag{2.2}$$

In the following often written as rapidity Y, which because in our case of nearly massless particles compared to their momentum ($\eta \approx Y$). 2.4 on the right side illustrates the new variable. Another variable that will be investigated in this is study is the centrality ζ. The definition was taken from the current implementation in CAF:

$$\zeta(l) = |\frac{\frac{1}{2}(Y_l) - (Y_{j_1} + Y_{j_2})}{\Delta Y_{jj}}| \tag{2.3}$$

The value depends on the rapidity of a single lepton relative to the tagging jets. The considered variable in the analysis is the centrality of the Z-boson $\zeta(Z)$, which is calculated by the centrality of the decay products via: $\zeta(Z) = max(\zeta(l_1), \zeta(l_2))$ Since its definition is not quite easy to understand, 4.1 shall give the idea. Here is the inverted definition used, where ζ grows as more central the detected boson is located with respect to the two jets. In this work the definition of formula 2.3 is used instead where ζ drops with a more central location.

3. Signal Significance

3.1. Significance Definitions

In high-energy physics and especially searching for new physics, there are possibilities to quantify experimental sensitivity. This is important to weight the analysis and draw conclusions. For the derivation of a significance definition, one needs a good background in statistics. For a more detailed comprehension refer to [7, 8]. This chapter shall explain the main idea, the application for the two different cases, and how its use in this study.
In statistical hypothesis testing, the significance can be determined in order to optimize a certain analysis. Starting with the null hypothesis, which is expected to be true. In particle physics, this is often defined as the well-known background, predicted by SM. The second step is formulating the alternative hypothesis, in the case of search for new physics, this would be the signal process. By analyzing measurements the question arises if the background hypothesis agrees with data or if it can be rejected.
At first, it's helpful to understand the idea of the p-value. In [7] its defined:

$$p_0 = \int_{t_{obs}}^{\infty} g(t/H_0)dt \tag{3.1}$$

$$p_1 = \int_{t_{obs}}^{\infty} g(t/H_1)dt \tag{3.2}$$

Whereat g(t/H) describes the probability density function of a test statistic of the respective hypothesis. In other words, the p-value gives the probability one would measure data, that is as far, or farther away, from the hypotheses as to the observed data t_{obs}. A small p-value implies that it's unlikely that the observed data corresponds to the hypotheses. This means the observation is more significant. The immediate link between p-value and significance Z can be expressed in the following formula [7]:

$$p = \frac{1 - erf(Z/\sqrt{2})}{2} \tag{3.3}$$

erf(x) is the error function. More concrete the relation can be seen in 3.1. So the significance grows with a lower p-value because it's less likely that the data is justified due to fluctuation of the considered theory.
Considering a counting experiment the significance can be evaluated and simplified [7, 8]:

$$Z = \frac{S}{\sqrt{B}} \tag{3.4}$$

with S being the number of signal events and B the number of background events. In this case, the null hypothesis equals the background-only hypothesis. This is used for observation of

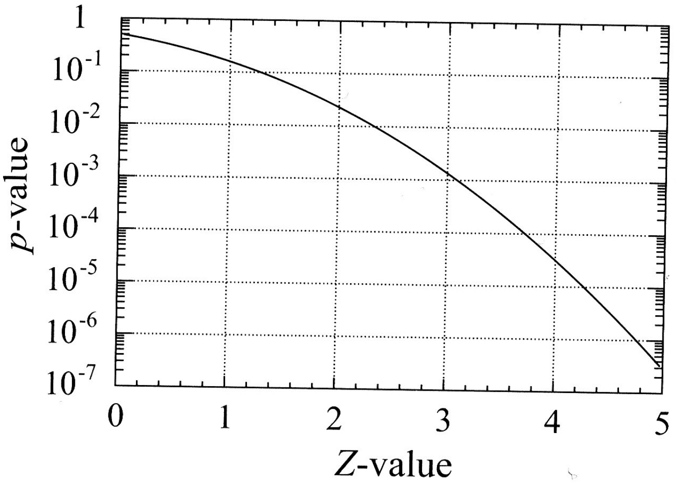

Abb. 3.1.: Descriptive correlation between the p-value and the significance Z [7]

new physics. It depends on how likely it is to measure S+B events when one expects only B events. Alternatively in analysis with the purpose of measurements and setting limits, one can invert the hypothesis. This significance depends on the likelihood that one measures B events when one expects S+B. Then the formula changes to:

$$Z = \frac{S}{\sqrt{S+B}} \tag{3.5}$$

The aim in resonance research is limit setting, which means excluding certain theories, see section 4.2.3. Therefore the second definition is more appropriate.

3.2. Optimizing phase spaces

The significance plot is the basic tool in this study, to find the optimal phase spaces. It has been implemented in CAF, the common analysis framework used by ATLAS. There is a subplot produced shown in 3.2. It tests different cuts on the respective variable. Then it merges all remaining events in one bin and calculates the significance defined in 3.4. The red and blue lines show the calculated significance for left- and right-handed cuts. The green line indicates the optimal range, with maximum significance.
Because of the impact of the mass of the resonance particle, there will be some discrepancy in this green line for different mass points. In the shown distributions 3.2 we get the range of interest of $m_{jj} > 700 GeV$ for GM225 and $m_{jj} > 1400 GeV$ for GM1000. Because one doesn't want to lose efficiency on lower masses, one chooses the area including all masspoints. In that case it would be $m_{jj} > 700 GeV$ which includes $m_{jj} > 1400 GeV$. This procedure will be done for all tested variables.
Recently there has been a new implementation of a limit significance plot in CAF. There the subplot uses the alternative definition of limit significance 3.5. Therefore the analysis has been iterated to see if the optimized phase spaces do change.

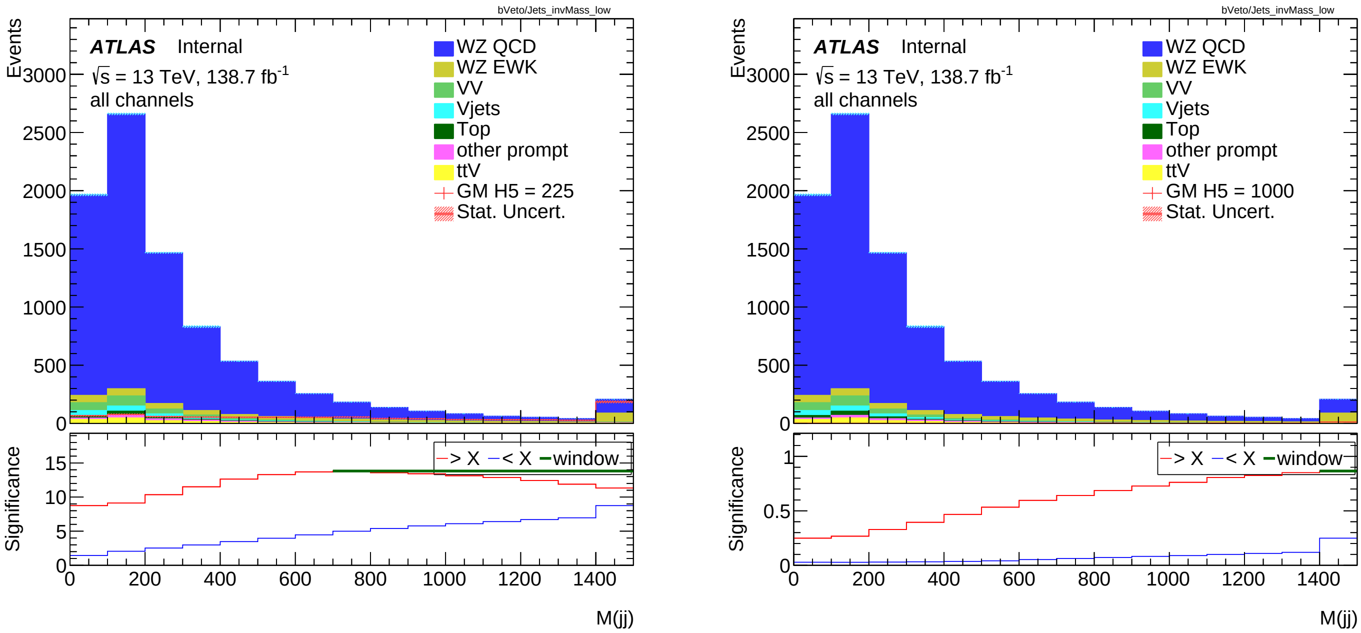

Abb. 3.2.: Distribution of event yields for invariant mass after bVeto selection, including significance subplot, for lowest GM225 (left) and highest masspoint GM1000 (right)

For validation of a new defined selection two figures of merit will be used. These are deviated by the significance definition in 3.5:

$$FoM1 = \frac{S}{\sqrt{S+B}} \tag{3.6}$$

$$FoM2 = \frac{S}{\sqrt{S+B+(0.3B)^2}} \tag{3.7}$$

Where both include statistical uncertainties, while the second formula also considers a 30% of the background, as systematic uncertainty. The results are shown in the next chapter describing the analysis.

4. Analysis and Results

Starting with the analysis, it's important to get an idea of current selections and why certain variables are considered. The typical behavior of the leptonic final state particles will be explained and what this implies for rapidity and mass. These properties are identical for each VBS/VBF process and are therefore summarised in the VBS/VBF topology. Based on the topology the current selection is introduced then. The analysis starts with the optimization of this nominal selection and afterward new variables will be considered and a different significance definition tested.

4.1. VBS/VBF topology

Due to the short lifetime of the interacting bosons, the VBF process in 2.2 need to take place in the hard process, which means immediately after the p-p collision. In the Feynman diagram, one can see each of the quark is radiating the bosons necessary for the fusion process. Due to the confinement, these will be detected later as the tagging jets. Since they only interact once by weak force their initial trajectories will only slightly change. This implies the azimuthal angular Θ will be very small for one and near maximum for the other jet. In other words, the rapidity difference ΔY_{jj} will be large. Additionally, the invariant mass of the two jets will be high compared to other possible processes. By looking at some background in the electroweak label see D, the quark will be produced here by the decay of a gauge boson, which results in a higher contribution in the lower mass section around 80-90 GeV. The third considered variable is the in section 3.3 introduced centrality. Illustrated in 4.1 the bosons are almost located central between the two jets. This implies that $\zeta(Z)$ from definition 2.3 needs to be small compared to background processes.

4.2. Cut-based optimization

The analysis aims to set new requirements on the phase space so the contribution of the signal grows relative to the number of background events. Validation occurs by calculating the two figures of merit definitions 3.6 and 3.7. Then they will be compared with previous selections and improvements are calculated. The study won't be restricted to currently used variables, but will also test new ones, which might have a good discrimination power. The cut-based optimization is realized with help of the significance plot, introduced in chapter 4, which was implemented in CAF. Since this subplot calculates the range with the maximum significance value, it will be used to determine the actual cut values, as explained in 4.2. To illustrate the mass dependence of the single variables, signals for the highest and lowest mass appropriate to the considered mass range have been investigated.

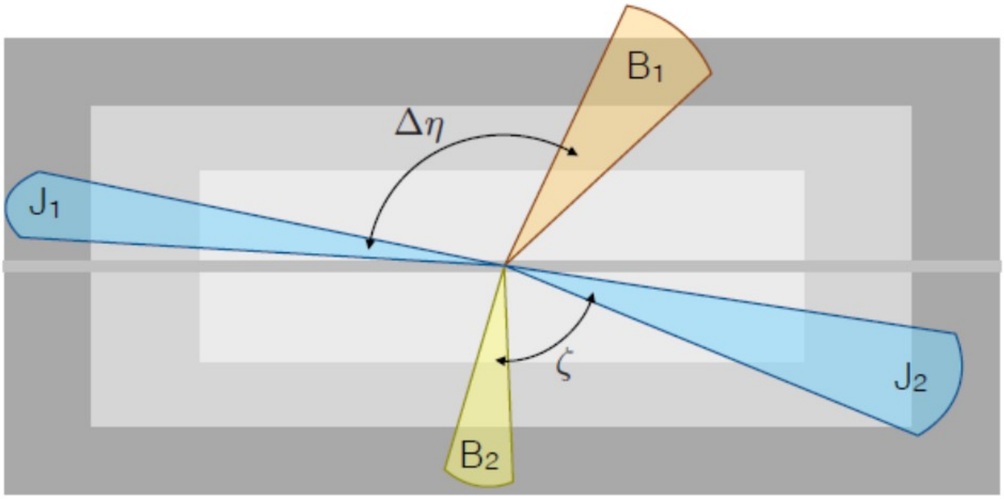

Abb. 4.1.: VBF topology for the two vector bosons and the tagging jets, with illustrated difference in pseudorapidity and centrality [9]

4.2.1. Current selection

For proving a certain theory, one needs to create a selection that enhances the signal contribution over the backgrounds. At first, a preselection is applied shown in Appendix E.1. This includes some quality requirements on the measurements of the detector, to reject background due to e.g. misidentified leptons. There are already cuts at certain variables, like the 20 GeV mass window around M(Z) mass. Further reduction of background is now realized by the selection applied on the signature variables for the VBF topology. At first events with the invariant mass of the two jets lower than 500 GeV were rejected. The second requirement is that the rapidity difference of the two jets needs to be larger than 3.5. The impact of the number of events of these cuts are presented in tables C.1 and C.2, shown for a mass of 225 (lowest) and 1000 GeV (highest). The first column labeled as bVeto represents the number of events before the two jet selection cuts but includes the preselection. The figures of merit are calculated and shown in the last two rows. One can see that the values increase significantly with each selection.

4.2.2. Optimization on typical VBF variables

Optimizing the cut values of the current selection, based on VBF topology, the distributions for lowest and highest masspoint of the invariant mass of tagging jets are considered A.1. One can see the mass dependence on the m_{jj} distribution for the signal. For a high mass of the $H_5^{\pm}$ particle the associated jets also have a higher mass contribution. The range with maximum significance has been calculated via the subplot. The new requirement on the jet mass is: $m_{jj} > 700 GeV$. The same is done for the rapidity difference between the jets ΔY_{jj} in A.2. The distribution includes the new m_{jj} cut. Analog with higher mass resonance particle the rapidity difference of the tagging jets grows. The new cut is applied at $\Delta Y_{jj} > 4.5$. This means for the optimization the cut values of the old selection have changed. Another variable from VBF topology, that wasn't considered in the analysis yet, is the centrality of the Z boson $\zeta(Z)$. The

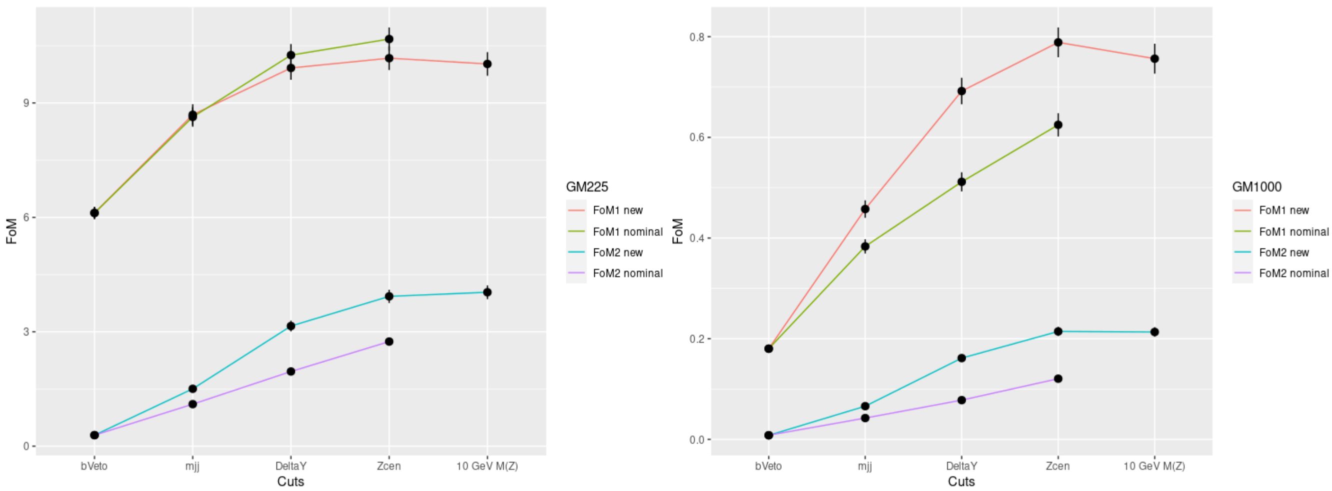

Abb. 4.2.: Plots for the improvements of the figures of merit of the nominal and new selection cuts applied for lowest mass 225 GeV (left) and highest mass 1000 GeV (right)

typical topology of the scattering process describes an incoming Z boson detected nearly mid between the two jets. These can be described by the centrality variable defined in 2.3. The associated distribution after the new selection of m_{jj} and ΔY_{jj} was created A.3. Looking at the plots one can notice, that especially for low centrality there is a huge signal contribution. The significance plot determines the new requirement of $\zeta(Z) < 0.4$.
The initial bVeto cut includes some preselection, including a 20 GeV cut around the mass of the Z boson $M(Z)$. This rejects background, where the associated lepton-antilepton pair do not originate from a Z boson. Without considering the significance plot a 10 GeV cut is tested instead. The number of events and figures of merit of all these new requirements can be seen in tables C.5, C.6.
Because of the good discrimination power and the consideration of implementing these new selections, there were some plots made to compare the improvement of the figures of merit. One wants to determine if it's worth applying the whole new selection or just add the new centrality requirement. Therefore there is a different centrality cut including the old selection applied. This corresponds to the case one keeps the current selection at m_{jj} and ΔY_{jj} and only adds the new $\zeta(Z)$ cut. The associated distribution is shown in A.4, with the equal range of interest of $\zeta(Z) < 0.4$. The associated number of events and the figures of merit were determined and presented in tables C.3, C.4. As validation these figures for each selection are additionally presented in the plots 4.2, also to see the improvement for each applied cut, again calculated for the lowest and highest masspoint. This shall help to answer the question, whether only the centrality cut will be added or the full new selection.
All possible selections improve the figures of merit. One can determine that the FoM2, which includes systematic uncertainties, improves the most with the new selection applied. For FoM1 the differences at 225 GeV are slight, while at 1000 GeV the improvements are again better with the new selection. The 10 GeV cut around Z mass does no significant improvement and will be excluded for further study. For the promising results, the relation of the improvements are shown in the summarizing table 4.1 as comparison between nominal and new selection. Additionally the percentage improvements when using the centrality cut only are shown here.

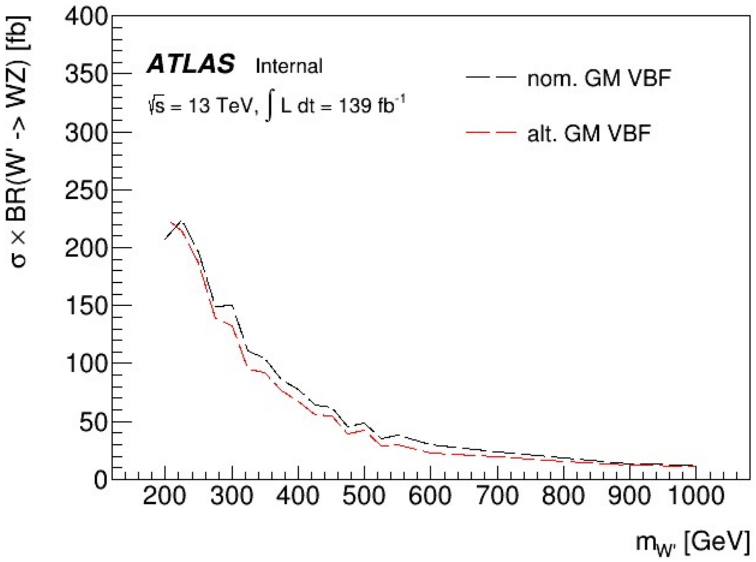

Abb. 4.3.: Comparison between exclusion limits for expected cross-section of nominal selection and alternative selection with additional centrality cut [10]

4.2.3. Exclusion limits with new centrality selection

Considering the good improvements with some of the new selections the WZ resonance group from ATLAS has decided to implement the new Z centrality requirement $\zeta(Z) < 0.4$ for their analysis. Therefore the exclusion limits for the new selection have been calculated. The comparison of the exclusion limits of the new and old selection was performed and is shown in 4.3. Understanding the proper meaning of these limits requires a good understanding of statistics similar to chapter 4. The section shall give an impression of its rough calculation. Considering the p-value defined in 3.1, the probability that the deviation of an observed number of events is due to fluctuation. Then we can define the confidence level (CL) [11]:

$$CL = 1 - p \tag{4.1}$$

For theories with higher signal contribution one may calculate the top limit s_{max} so that $p_{S+B} > 0.05$. These were determined for all the different masspoints. Knowing the integrated luminosity s_{max} may be converted to cross-section limit σ_{max}. By looking at the plot one can see that the red line with the new centrality requirement is lower than the black line for the nominal selection. This means one has a tighter area of possible models. In other words, one can exclude more high cross-section theories. This shows once again the benefit of this new centrality selection for the analysis.

4.2.4. Investigating new variables

Besides the common phase spaces one uses to separate the signal from the background, there will be some new variables tested. At first, the rapidity difference between the W and Z boson has been investigated, and the distribution is shown in A.5. Due to the less good discrimination between background and the 1000 GeV signal, one can not define a new requirement sensitive

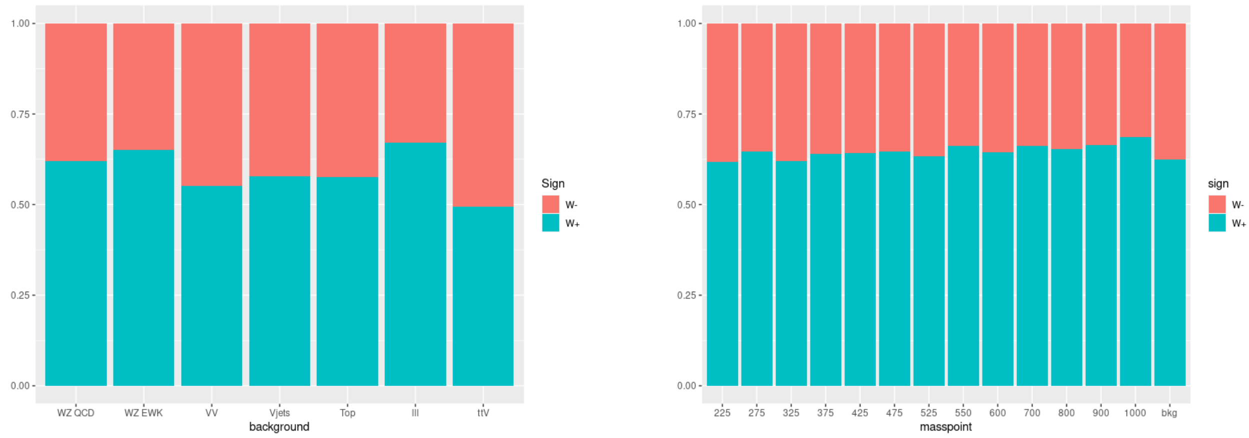

Abb. 4.4.: Relative fraction of event numbers for W^+ and W^- contribution, for the different backgrounds (left) and signal masspoints (right)

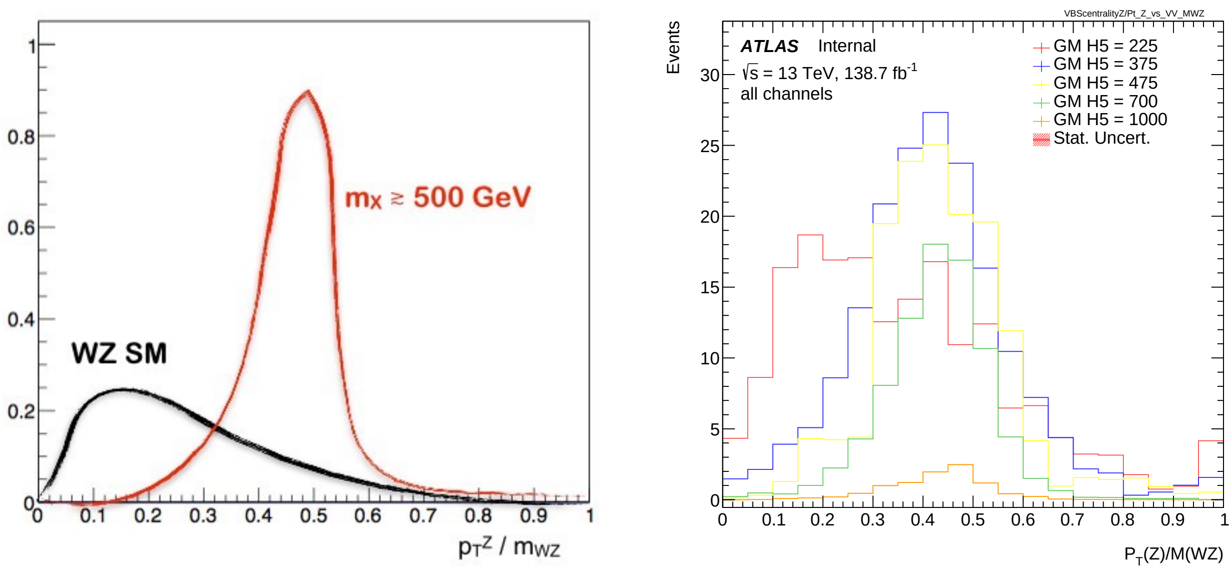

Abb. 4.5.: $p_T(Z)/M(WZ)$ distribution for some generated masspoints (right) and for the expected contributions for high mass signal and WZ SM background (left) [9]

to all masses. Because of the known asymmetry of W^{*} and W^{-} production, these distributions have been tested separately. The associated $\Delta Y(WZ)$ for both signs are created separately for 225 GeV A.6 and 1000 GeV A.7 after the completely new requirements of m_{jj}, ΔY_{jj}, $\zeta(Z)$. There is no selection possible for both variables by using the subplot. Closing the study on the variable there was a plot made, representing the relative fraction of W^{+} and W^{-} for the single background and signal contributions in 4.4.
The plot agrees with predictions, 60 % W^{+} and 40 % W^{-} contribution for WZ SM background, related to the parton density function, more precisely described in [12].
Furthermore new examined variables like the transverse momenta relative to the invariant mass of W and Z boson $p_T(Z/M(WZ)Z$, $p_T(W)/M(WZ)$, the scalar sum of all leptons transverse momenta L_T and the difference in polar angles between missing transverse energy and W boson $\Delta\Phi(l^W, E_T^{miss})$ distributions after new centrality selection are tested in A.8, A.9, A.10, A.11. Especially for the low mass distribution of 225 GeV , one can distinguish that all these variables have less good discrimination power considering all masspoints. For that reason the different signals were labeled in low and high masspoints, so one may optimize for them separately.
This classification is conversed by declaring certain masspoints as boosted, which means the associated resonance particle wasn't produced at rest. This immediately depends on its mass, since for high mass resonances it's more likely that the fused bosons need to invest the whole energy to produce the new particle, but without any kinetic energy. In that case, the decay products will split the energy from the rest mass into their own mass and momentum. Since we only consider transverse momentum one should still see a peak approximately around 0.5 for the $p_T(Z)/M(WZ)$ distribution for the signal process like in 4.5 on the left. The other plot on the right presents the $p_T(Z)/M(WZ)$ distribution generated for some signal samples with different masses. This confirms the theory that the higher mass contributions center around 0.5. To distinguish between a low and high mass the following study is performed. Therefore a cut at $p_T(Z)/M(WZ) > 0.3$ is applied. The number of events and the relative ratio before and after the cut are determined for each masspoint. The ratio was calculated for each masspoint and is illustrated in the plot in 4.6. Based on that, the low mass range 225 - 425 GeV and high mass range 475 - 1000 GeV were defined.
Equivalently to the previous optimization, one can now optimize with help of the significance plot. For investigating the high mass classification again the lowest and highest masses are considered, i.e. 475 GeV and 1000 GeV. The associated distributions are tested for the high mass range A.12, A.13, A.14, A.15. The consequential cuts are applied in the following order: $p_T(Z)/M(WZ) > 0.3$, $p_T(W)/M(WZ) > 0.25$, $L_T > 250GeV$, $\Delta\Phi(l^W, E_T^{miss} < 1.2$ Whereat one can presume by looking at $\Delta\Phi$ distribution that the latest selection won't have a great impact on optimization, since there is almost no background rejected.
The associated tables with the number of events and figures of merit for lowest and highest mass are given in C.7, C.8. The plots with improvements for the two figures of merit are shown in 4.7 for both masspoints . The improvements are looking good especially for the highest mass of 1000 GeV.
Because the analysis needs to be sensitive to all possible masses, one needs to include masspoints between 225 and 425 GeV as well. For these, the resonance particle is considered as boosted due to its low mass. By defining the high mass signal region by the selection mentioned before, one determines simultaneously the orthogonal low mass region requirements. The

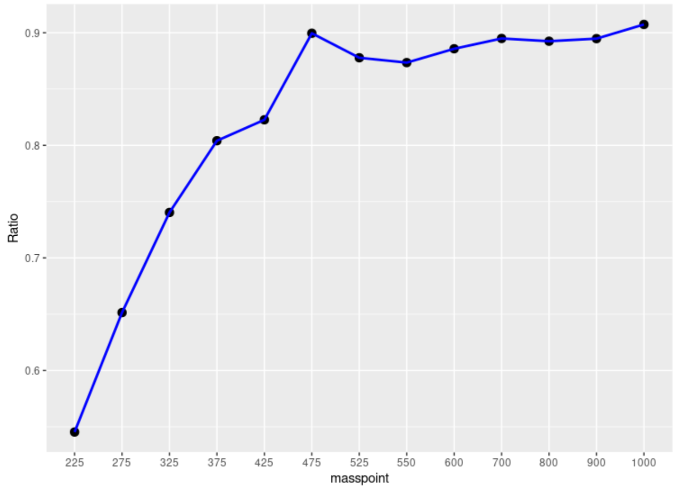

Abb. 4.6.: Fraction of events after the $p_T(Z)/M(WZ) > 0.3$ cut relative to number before the cut, calculated for all possible masspoints

cuts and associated number of events and the figures of merit are presented in tables C.9, C.10, again for the lowest and highest masspoints of 225 and 425 GeV. By looking at the plots of improvements 4.8, one can see that especially in that low mass range one looses a lot of signal contribution compared to the background. Which means one looses a lot of sensitivity here. Since the mass of the resonance particle $H_5^\pm$ is unknown the selection on the new variables seems inappropriate. Table 4.1 illustrates impressive the benefit on high mass compared to the decrease at low mass signals.

4.2.5. Testing limit Significance

The dependence of the used significance definition on the optimization results is investigated. As mentioned before, the goal in resonance analysis and phase space optimization is limit setting, to exclude certain theories (Section 4.2.3). However, the previous cut-based optimization uses the observation definition of $Z = S/\sqrt{B}$. Lately, there has been a new implementation of a limit significance subplot in CAF. Therefore the analysis was repeated analogously with the new definition $Z = S/\sqrt{S+B}$ used. Because the new m_{jj}, ΔY_{jj} and $\zeta(Z)$ selection seems the most promising, these will be tested with the limit significance subplot again.
The variables are investigated in the same order as previously. The distributions are shown in B.1, B.2, B.3. Analog to section 4.2.2 the centrality cut was optimized for the nominal selection in B.4. The tables in C.11, C.12, C.13, C.14 shall serve as a comparison between the selections. The plots for the FoM's improvements were created and are illustrated in 4.9.
Regarding the studies, one can see, that the cut-values change slightly with the new significance definition. By comparing the FoM's in the tables, the cut values defined by limit significance are slightly higher for each variable. But this is just a small benefit, so the original significance plot is still a useful tool to optimize the selection. The percentage improvements for the new selection compared to the nominal are shown in table 4.2.

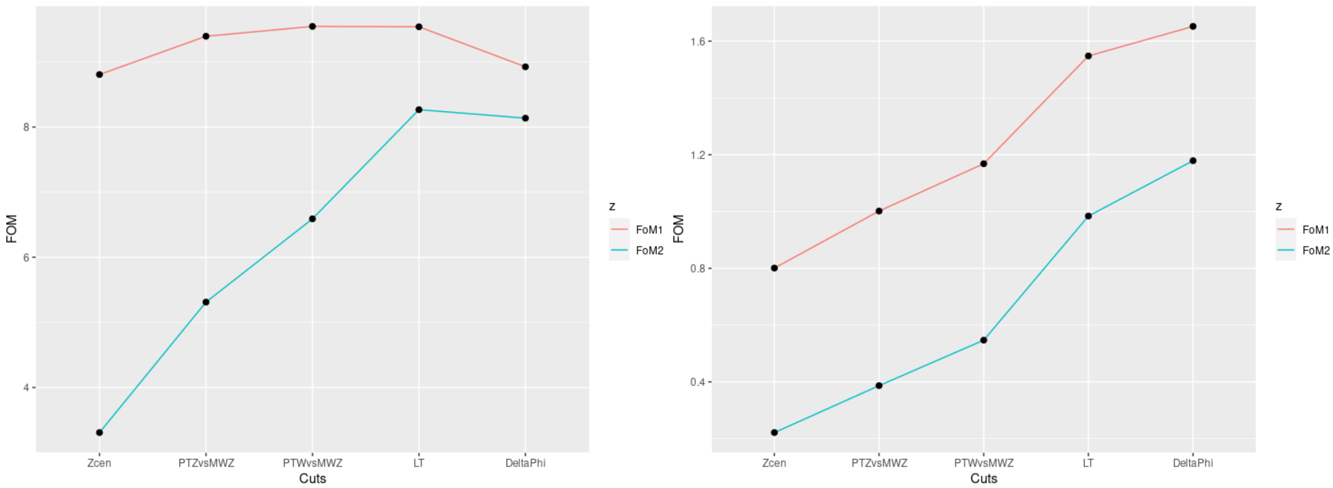

Abb. 4.7.: Plots for the improvements of the figures of merit of the new selection cuts applied for high mass signal range, lowest mass 475 GeV (left) and highest mass 1000 GeV (right)

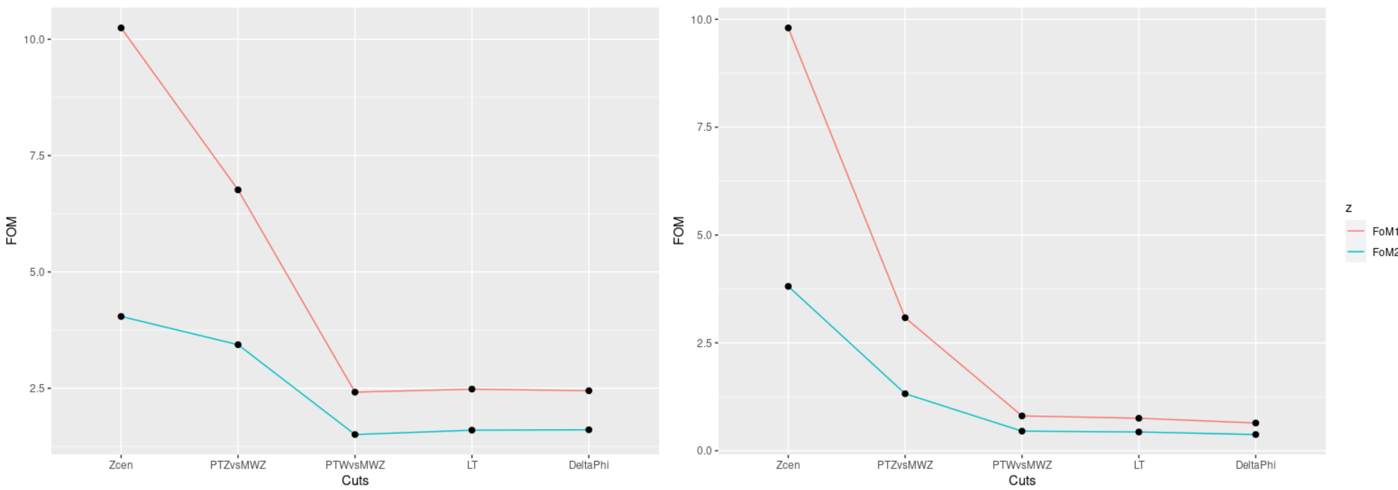

Abb. 4.8.: Plots for the improvements of the figures of merit of the new selection cuts applied for low mass signal range, lowest mass 225 GeV (left) and highest mass 425 GeV (right)

new selection	masspoint	Improvements	
		FoM1	FoM2
centrality cut only	225	4.108 ± 4.172%	40.088 ± 7.573%
	1000	22.122 ± 6.399%	54.615 ± 8.788%
with additional mjj and Delta Yjj	225	−0.788 ± 4.130%	100.644 ± 11.578%
	1000	54.133 ± 8.138%	175.000 ± 15.987%
new variables	225	−76.134 ± 2.775%	−17.889 ± 11.409%
	1000	222.865 ± 16.647%	1411.667 ± 88.419%

Tab. 4.1.: Percentage improvements of the figures of merit for the new selections calculated for different masspoints compared to the current selection of $m_{jj} > 500 GeV$ and $\Delta Y_{jj} < 3.5$, for nominal significance definition

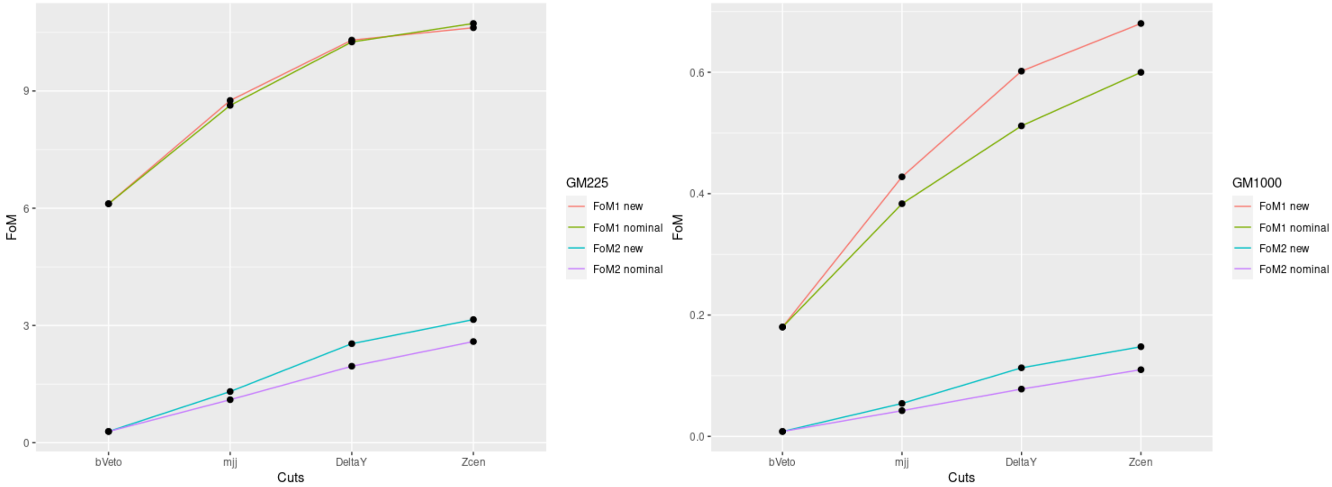

Abb. 4.9.: Improvements of the figures of merit of the nominal and new selection cuts (limit significance used), applied for lowest mass 225 GeV (left) and highest mass 1000 GeV (right)

new selection	masspoint	Improvements	
		FoM1	FoM2
centrality cut only	225	4.615 ± 2.998%	32.232 ± 7.094%
	1000	17.237 ± 6.146%	40.897 ± 7.949%
with additional mjj and Delta Yjj	225	3.558 ± 4.190%	60.980 ± 8.907%
	1000	32.969 ± 6.988%	89.487 ± 10.857%

Tab. 4.2.: Percentage improvements of the figures of merit for the new selections calculated for different masspoints compared to the current selection of $m_{jj} > 500GeV$ and $\Delta Y_{jj} < 3.5$, for limit significance definition

5. Conclusion and Summary

Resonance searches are one of the simplest way to look for physics Beyond the SM using data. In this thesis the phase space selection was optimized to reduce the background contributions to the search. This affects at the end the significance and helps to decide whether the data agree with the SM or a new physics theory. With the statistical approach over the significance, one can evaluate this purpose in numbers.
For that reason, the typical variables m_{jj}, ΔY_{jj}, $\zeta(Z)$ of VBS topology have been investigated. This makes the study also sensitive to SM since the predicted triple and quartic coupling processes and their signals may profit from this adjusted selection. New cut values have been determined via significance subplot and the figures of merit of nominal and new selection were calculated to see the improvements. Especially the new centrality requirement appears to have good discrimination power. Therefore improvements have been compared to see, whether a completely new selection with optimized m_{jj} and ΔY_{jj} cuts or only new $\zeta(Z)$ requirement is worth applying for prospective studies. The resonance workgroup decided to implement the centrality selection and calculated some exclusion limits for the current and the new selection. The associated plot illustrated the use of the new selection which allows to reject certain theories with high cross-section.
In the second step some, completely new variables that haven't been considered yet were investigated. Here the $\Delta Y(WZ)$ variable was tested. No selection criteria was defined and the distributions with W^+ and W^- contribution were considered separately. The samples agreed with a 60%/40% ratio between the contributions like the predictions. Additionally the distributions of $p_T(Z)/M(WZ)$, $p_T(W)/M(WZ)$, L_T and $\Delta\Phi(E_T^{miss}, l_W)$ were investigated. Here the strong dependence of the resonance particle mass was problematic for a common signal region. So the masspoints were grouped depending on whether the $H_5^{\pm}$ is boosted or not. A high mass range between 475 and 1000 GeV and a low mass range between 225 and 425 GeV was defined. The optimization was performed analog to the previous analysis for the high masspoints. The corresponding improvements of the figures of merit looked quite good especially for the highest mass of 1000 GeV. Since the mass of the predicted resonance in the GM model is unknown, the study must be sensitive to all masspoints. The orthogonal phase space has been assigned to the lower masses. Here a strong decrease of the figures of merit was observed.
The last part has profited from the recent implementation in CAF. The new formula was used to calculate the limit significance for the merged bins. For resonance research and limit setting, this has been the appropriate definition. For that reason, part one of the study, investigating variables from VBF topology, including the promising centrality selection, was repeated. The optimization was performed and improvements were calculated again via figures of merit. The results show that the cut values will change by using the new definition. Also the validating figures of merit improve slightly. The effect seems relatively small, so the nominal significance definition seems furthermore a useful tool for validating signal regions.

Appendix

A. Distributions- with nominal significance subplot

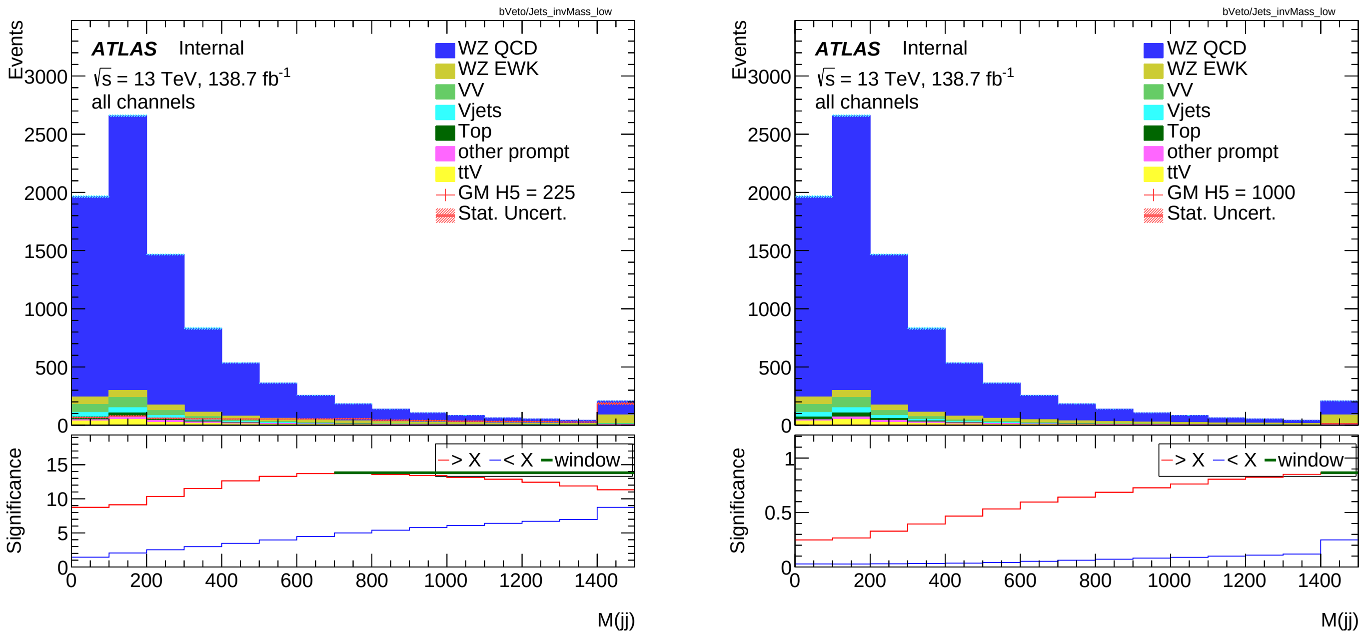

Abb. A.1.: Distribution of event yields for invariant mass after bVeto selection, including significance subplot, for lowest GM225 (left) and highest masspoint GM1000 (right)

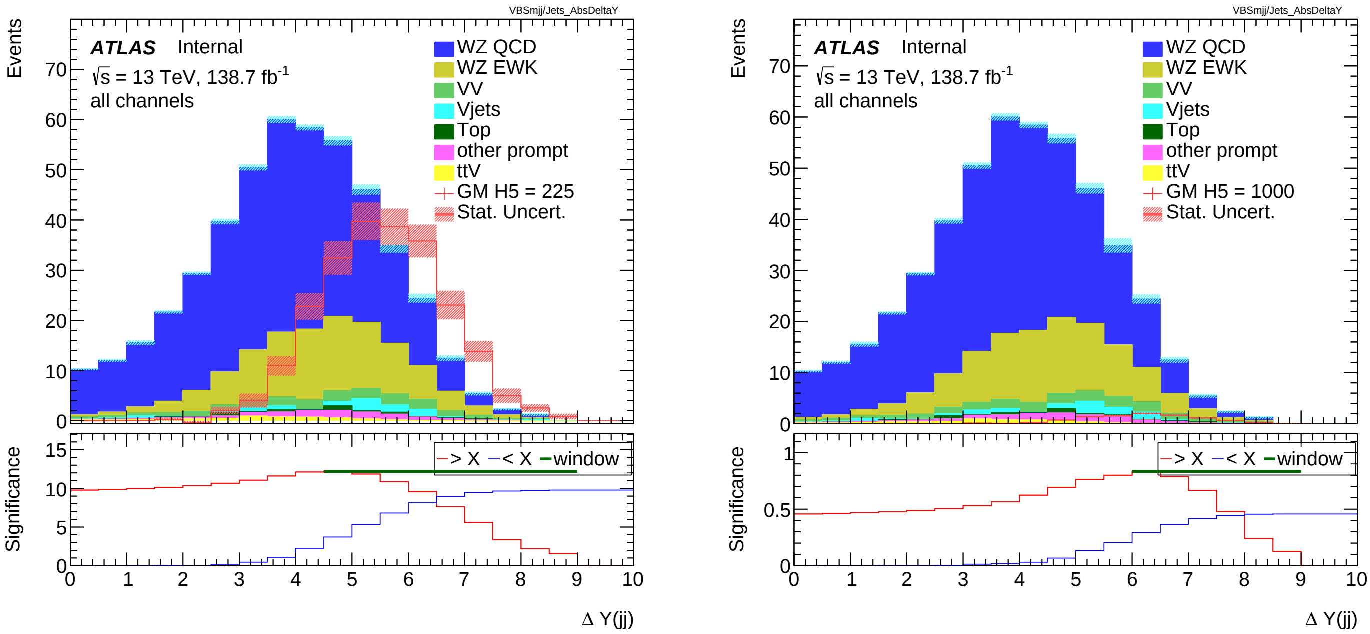

Abb. A.2.: Distribution of event yields for rapidity difference of the tagging jets after new m_{jj} selection, including significance subplot, for lowest GM225 (left) and highest masspoint GM1000 (right)

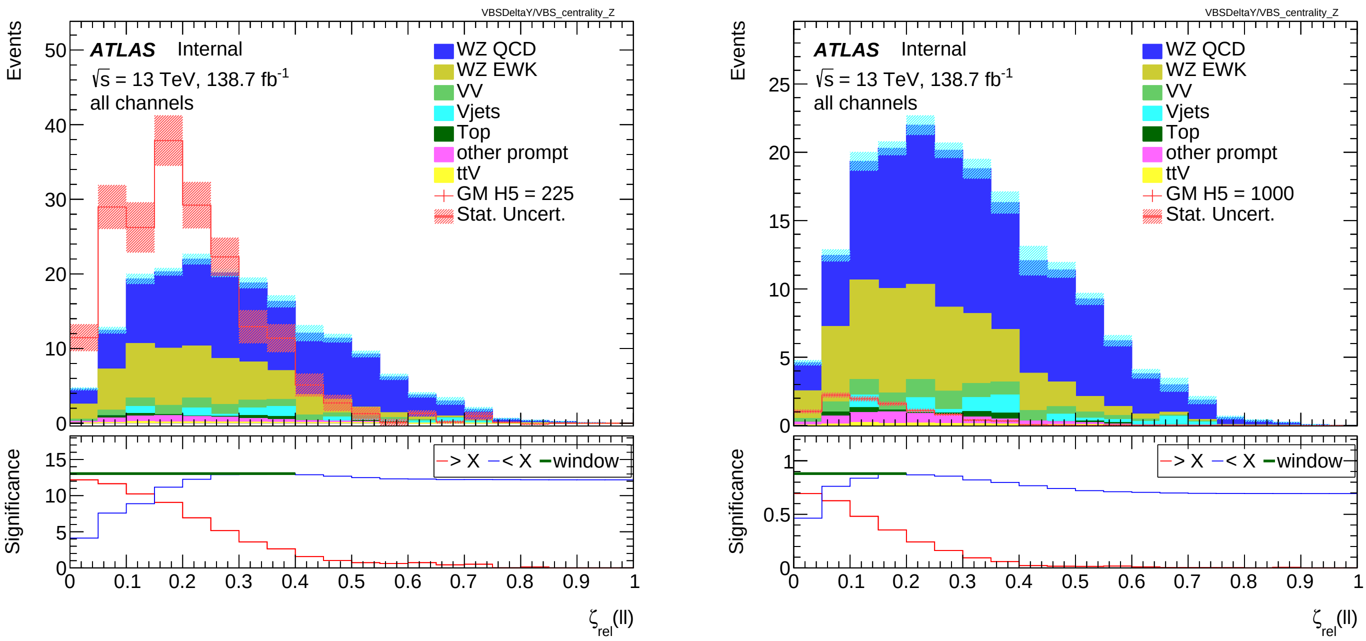

Abb. A.3.: Distribution of event yields for Z centrality after new ΔY_{jj} selection, including significance subplot, for lowest GM225 (left) and highest masspoint GM1000 (right)

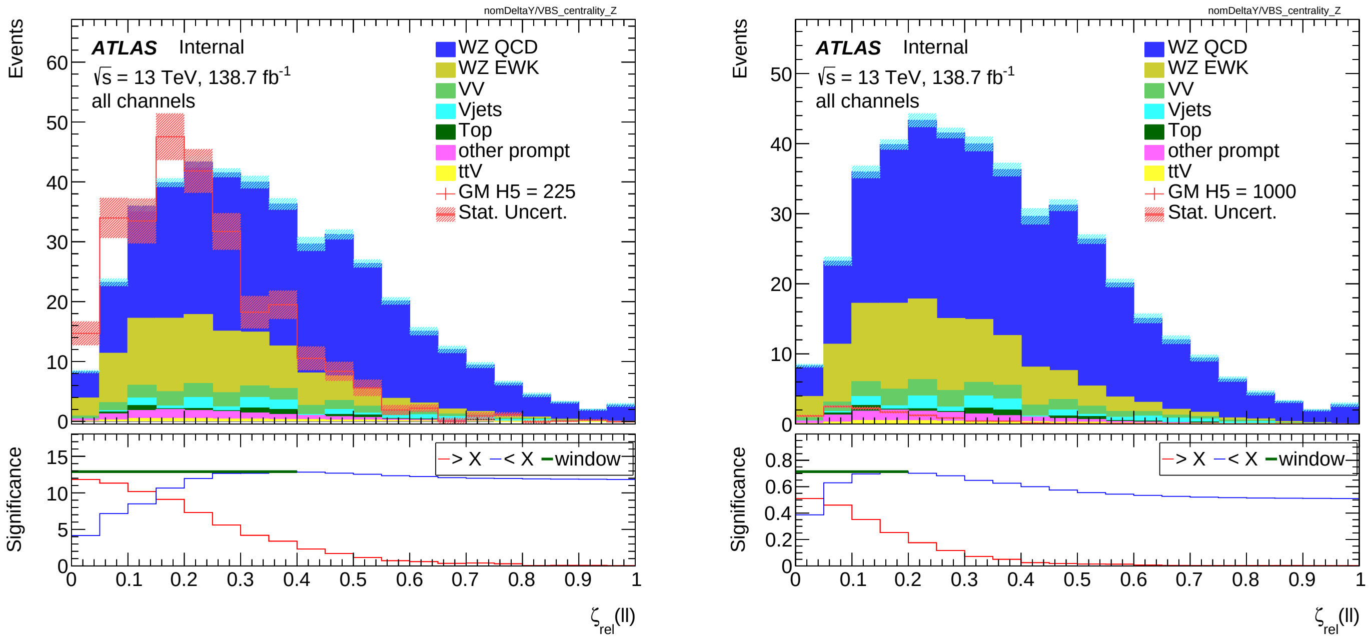

Abb. A.4.: Distribution of event yields for Z centrality after nominal m_{jj} and ΔY_{jj} selection, including significance subplot, for lowest GM225 (left) and highest masspoint GM1000 (right)

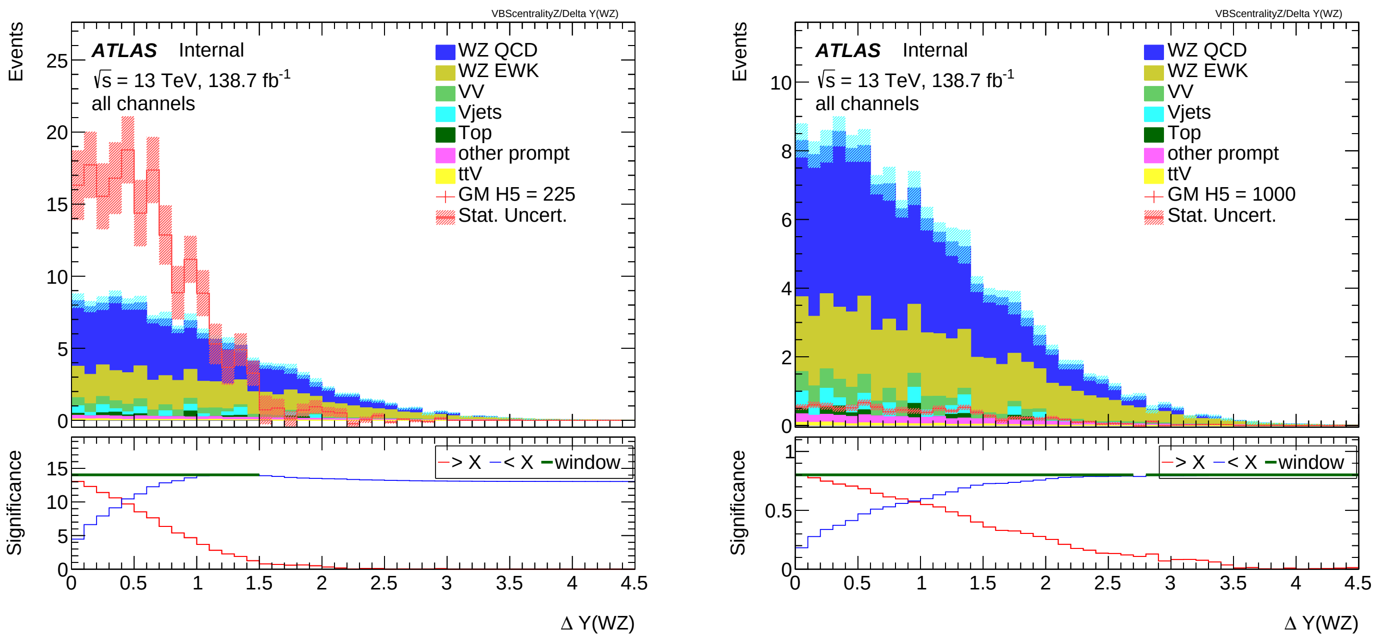

Abb. A.5.: Distribution of event yields for rapidity difference between the W and Z boson after new $\zeta(Z)$ selection, including significance subplot, for lowest GM225 (left) and highest masspoint GM1000 (right)

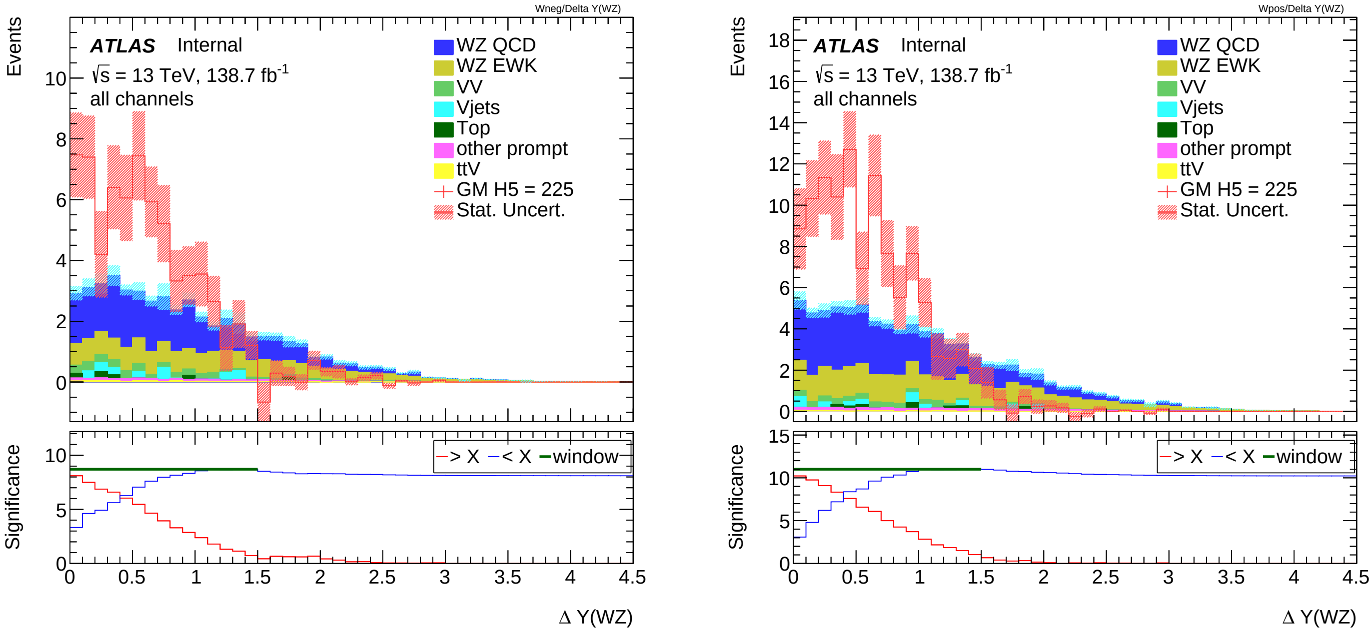

Abb. A.6.: Distribution of event yields for rapidity difference between the W and Z boson after new $\zeta(Z)$ selection, including significance subplot, for W^- (left) and W^+ contribution (right) with lowest masspoint GM225

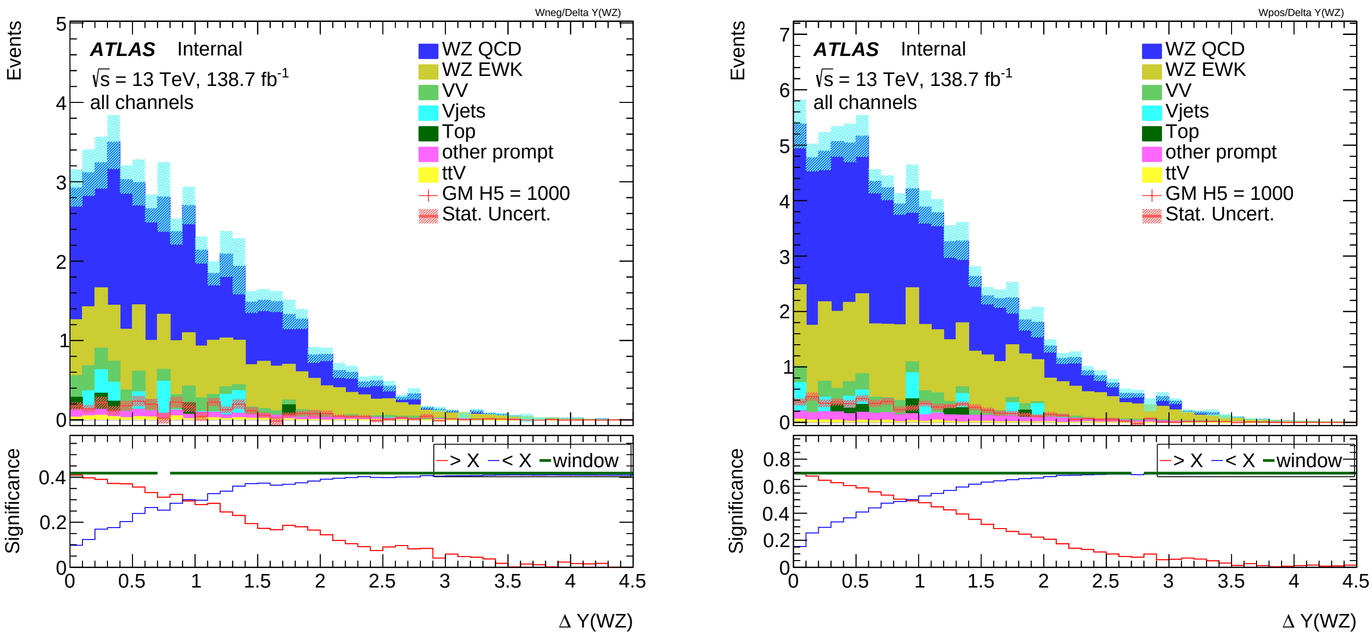

Abb. A.7.: Distribution of event yields for rapidity difference between the W and Z boson after new $\zeta(Z)$ selection, including significance subplot, for W^- (left) and W^+ contribution (right) with highest masspoint GM1000

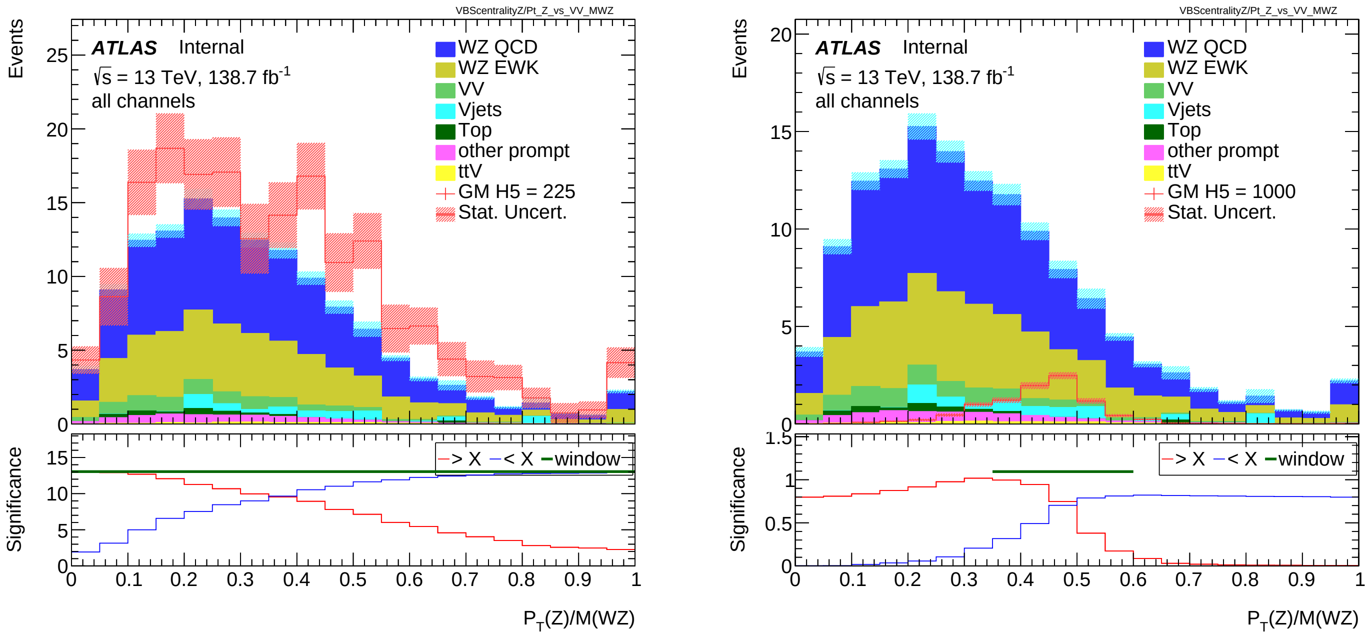

Abb. A.8.: Distribution of event yields for ratio between transverse momentum of Z boson and invariant mass M(WZ) after new $\zeta(Z)$ selection, including significance subplot, for lowest masspoint GM225 (left) and highest masspoint GM1000 (right)

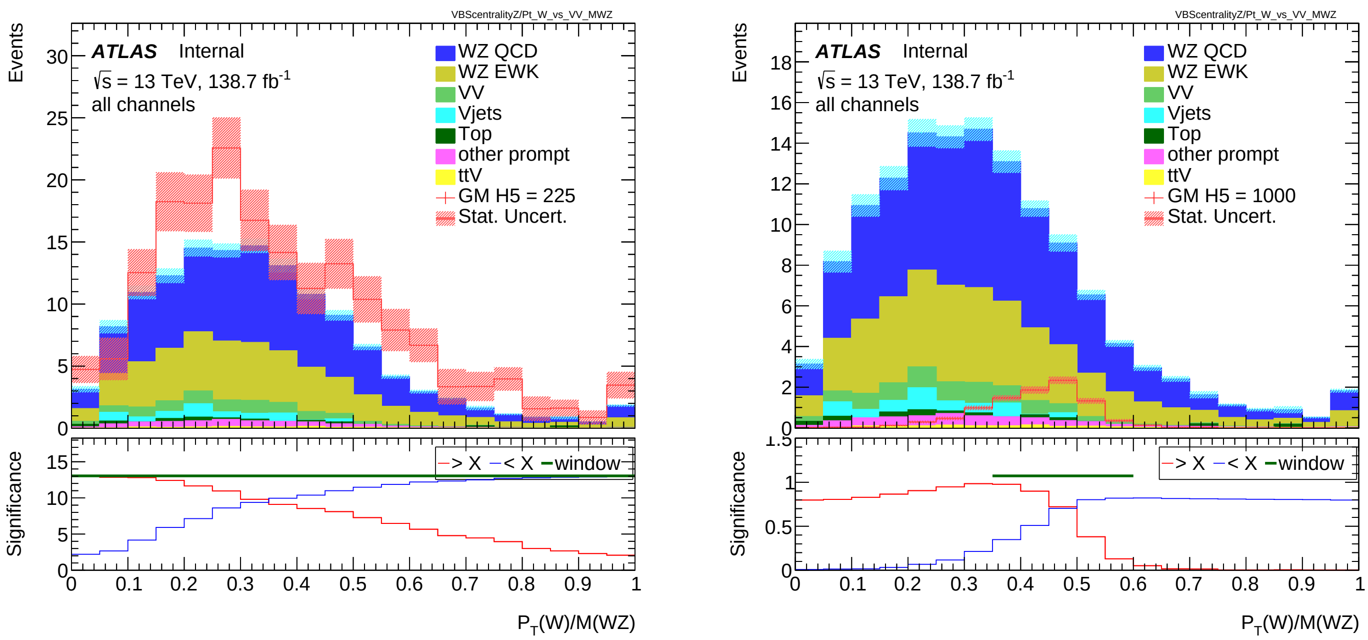

Abb. A.9.: Distribution of event yields for ratio between transverse momentum of W boson and invariant mass M(WZ) after new $\zeta(Z)$ selection, including significance subplot, for lowest GM225 (left) and highest masspoint GM1000 (right)

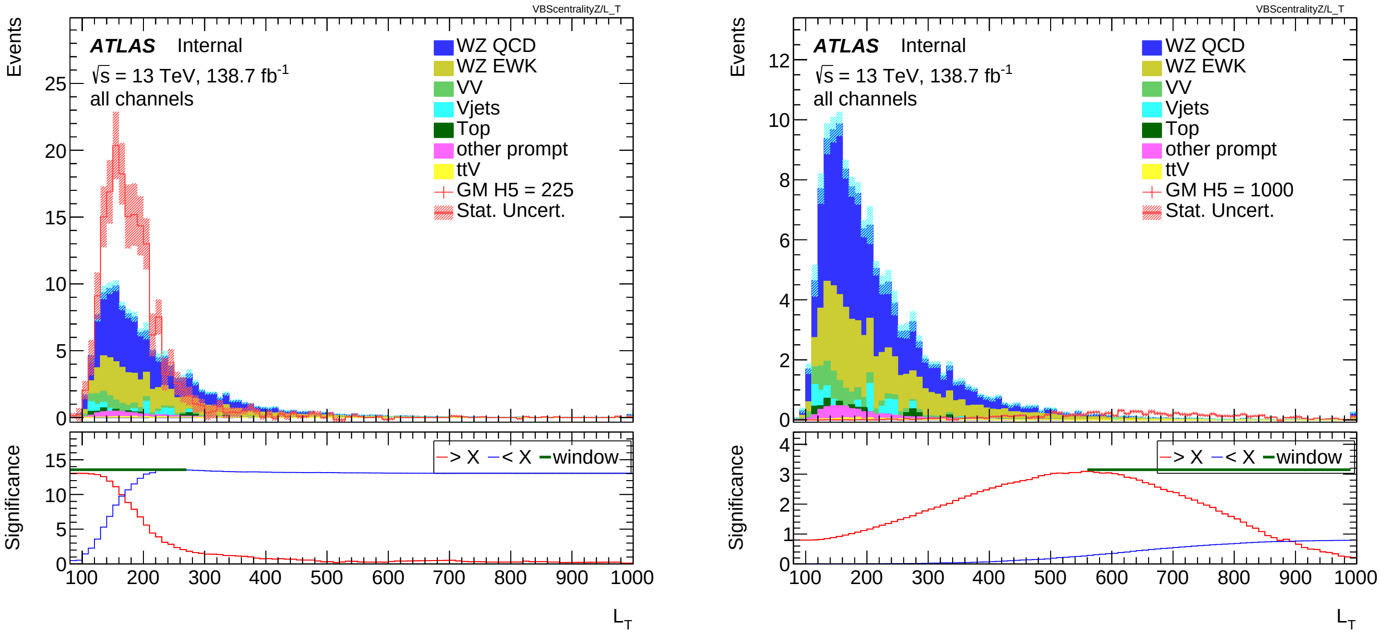

Abb. A.10.: Distribution of event yields for scalar sum of all leptons transverse momentum after new $\zeta(Z)$ selection, including significance subplot, for lowest GM225 (left) and highest masspoint GM1000 (right)

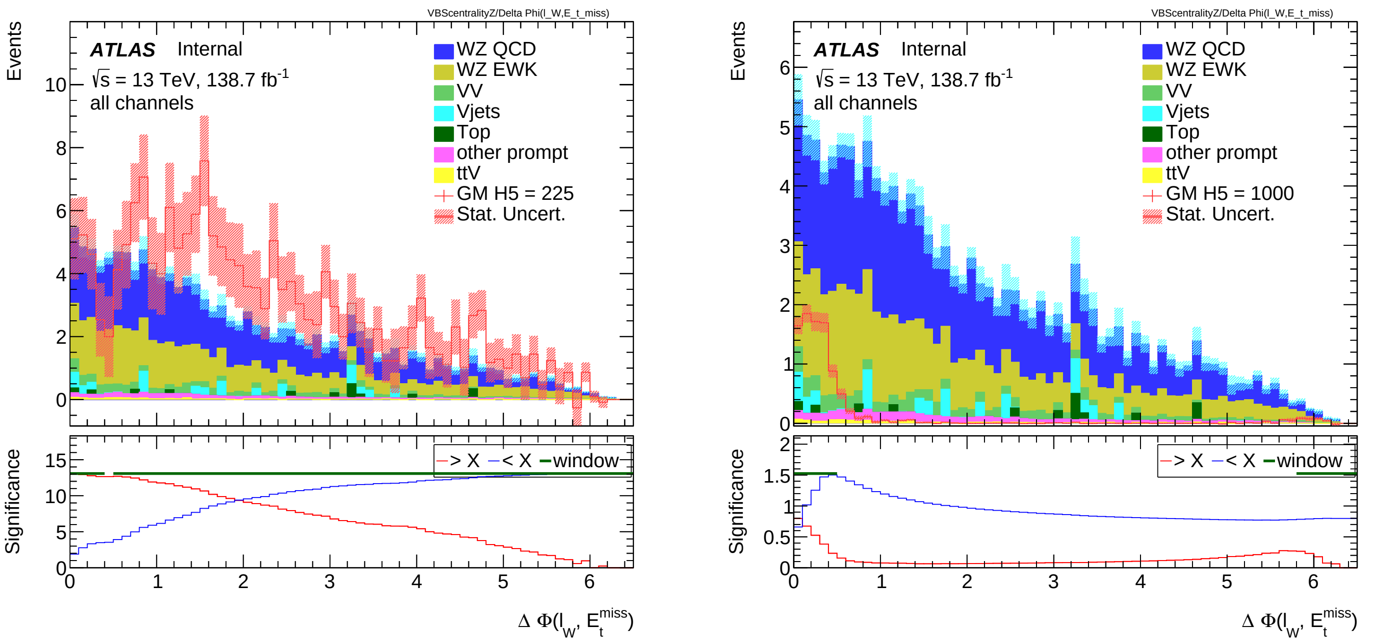

Abb. A.11.: Distribution of event yields for difference between polar angles of the lepton associated to the W boson and the transverse missing energy (neutrino) after new $\zeta(Z)$ selection, including significance subplot, for lowest GM225 (left) and highest masspoint GM1000 (right)

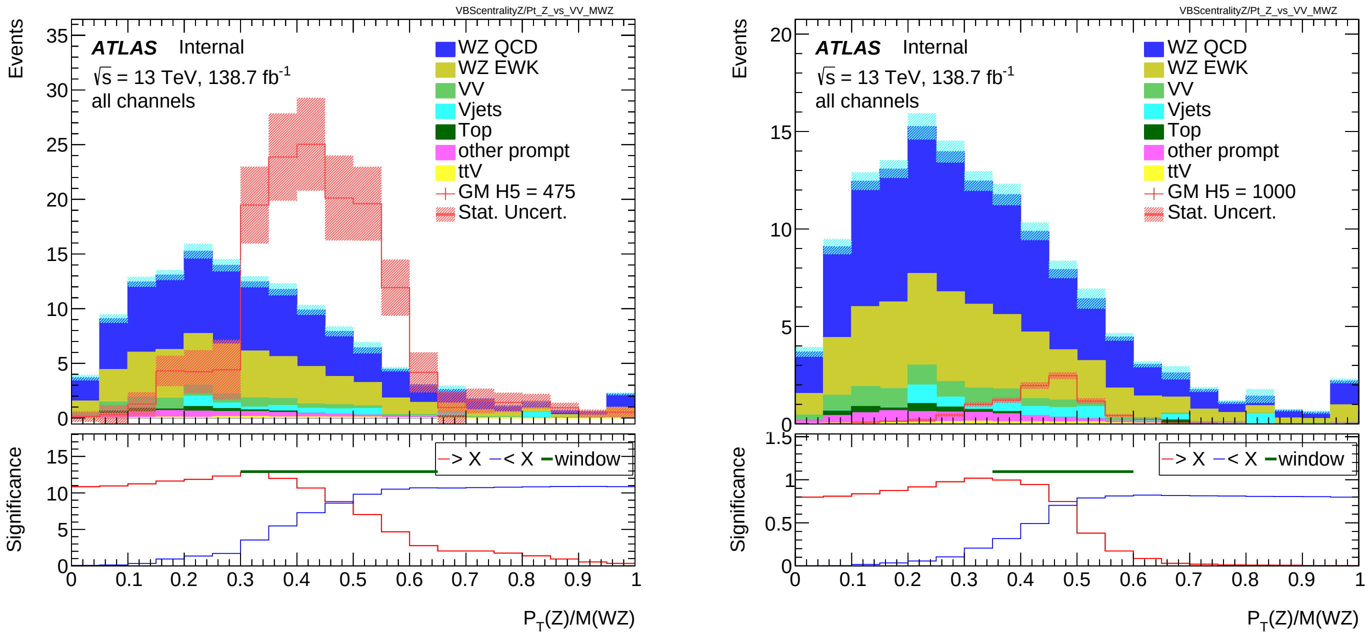

Abb. A.12.: Distribution of event yields for ratio between transverse momentum of Z boson and invariant mass M(WZ) after new $\zeta(Z)$ selection, including significance subplot, for lowest GM475 (left) and highest masspoint GM1000 (right)

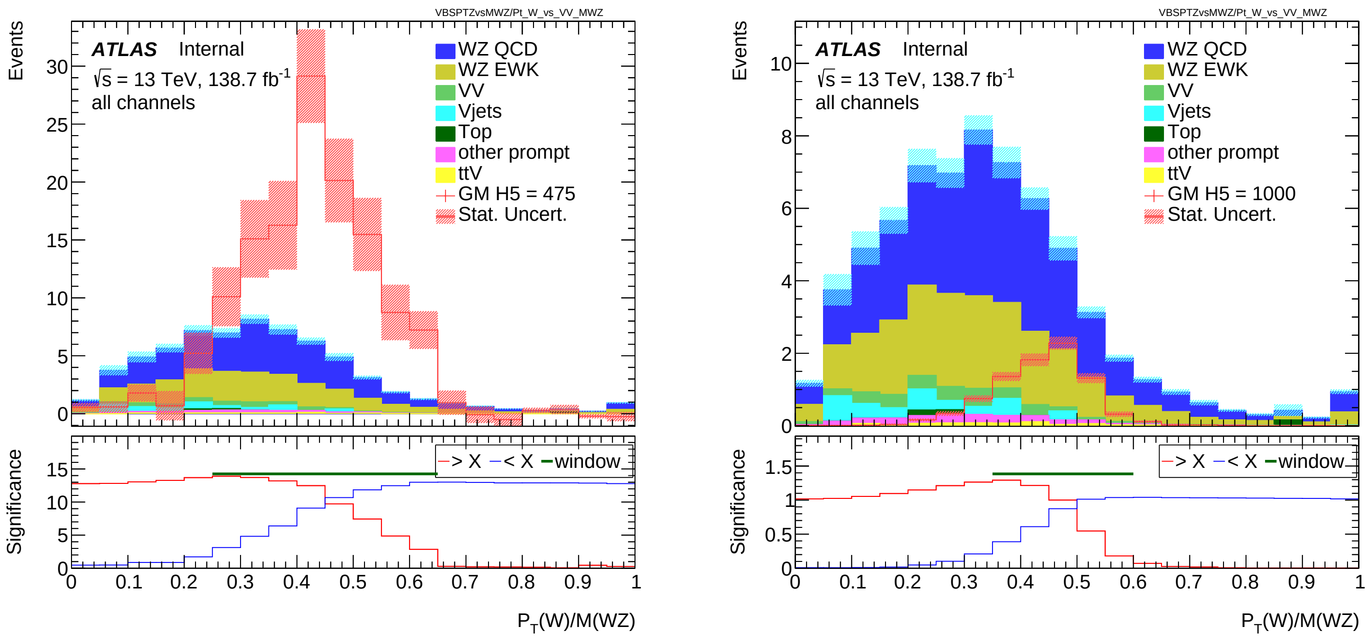

Abb. A.13.: Distribution of event yields for ratio between transverse momentum of W boson and invariant mass M(WZ) after new $p_T(Z)/M(WZ)$ selection, including significance subplot, for lowest GM475 (left) and highest masspoint GM1000 (right)

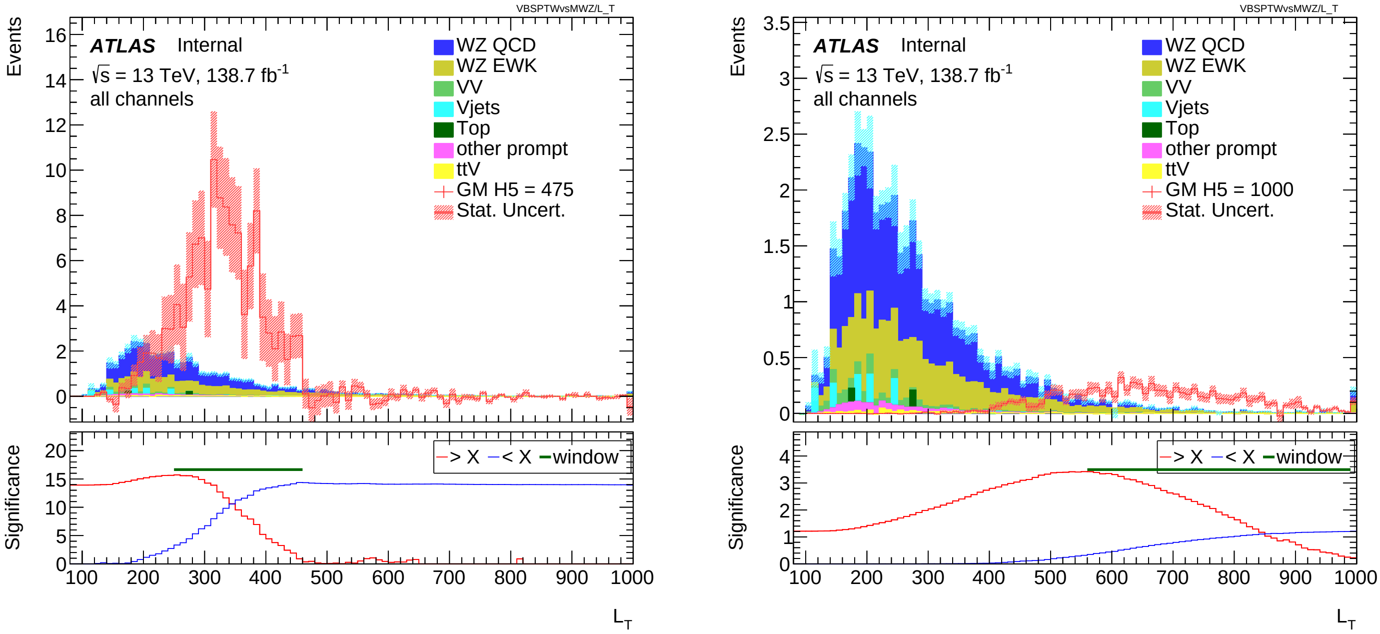

Abb. A.14.: Distribution of event yields for scalar sum of all leptons transverse momentum after new $p_T(W)/M(WZ)$ selection, including significance subplot, for lowest GM475 (left) and highest masspoint GM1000 (right)

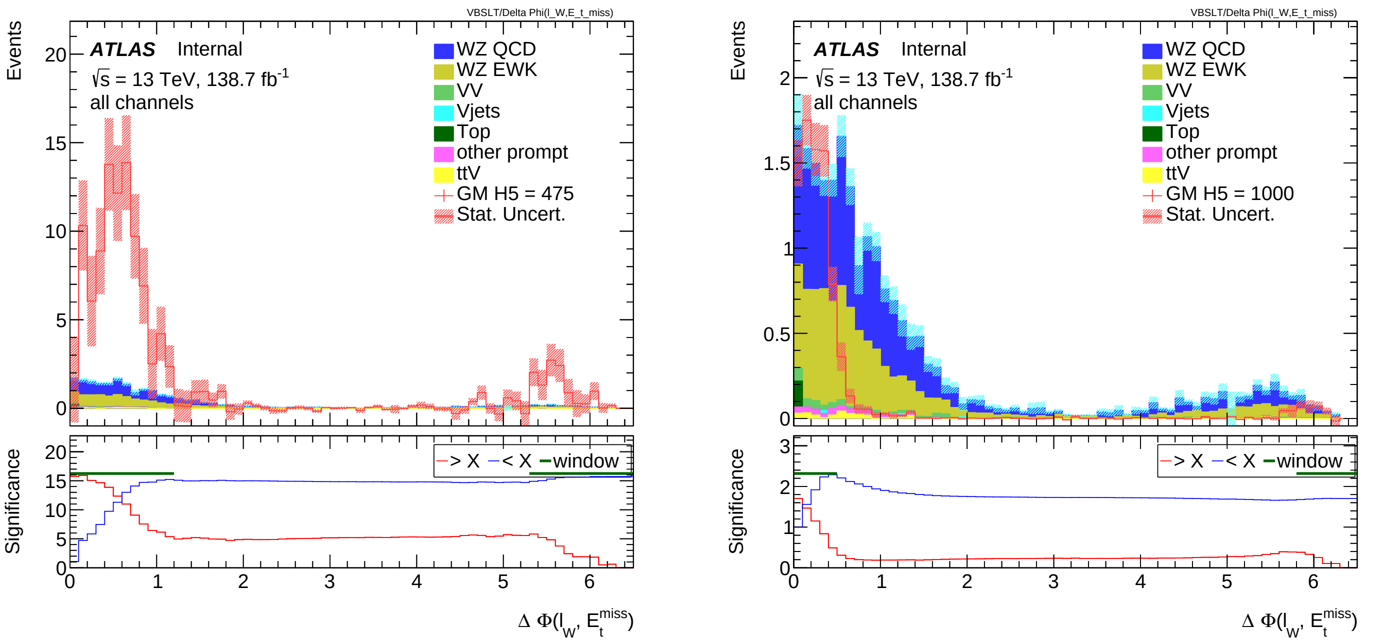

Abb. A.15.: Distribution of event yields for difference between polar angles of the lepton associated to the W boson and the transverse missing energy (neutrino) after new L_T selection, including significance subplot, for lowest GM475 (left) and highest masspoint GM1000 (right)

B. Distributions - with limit significance subplot

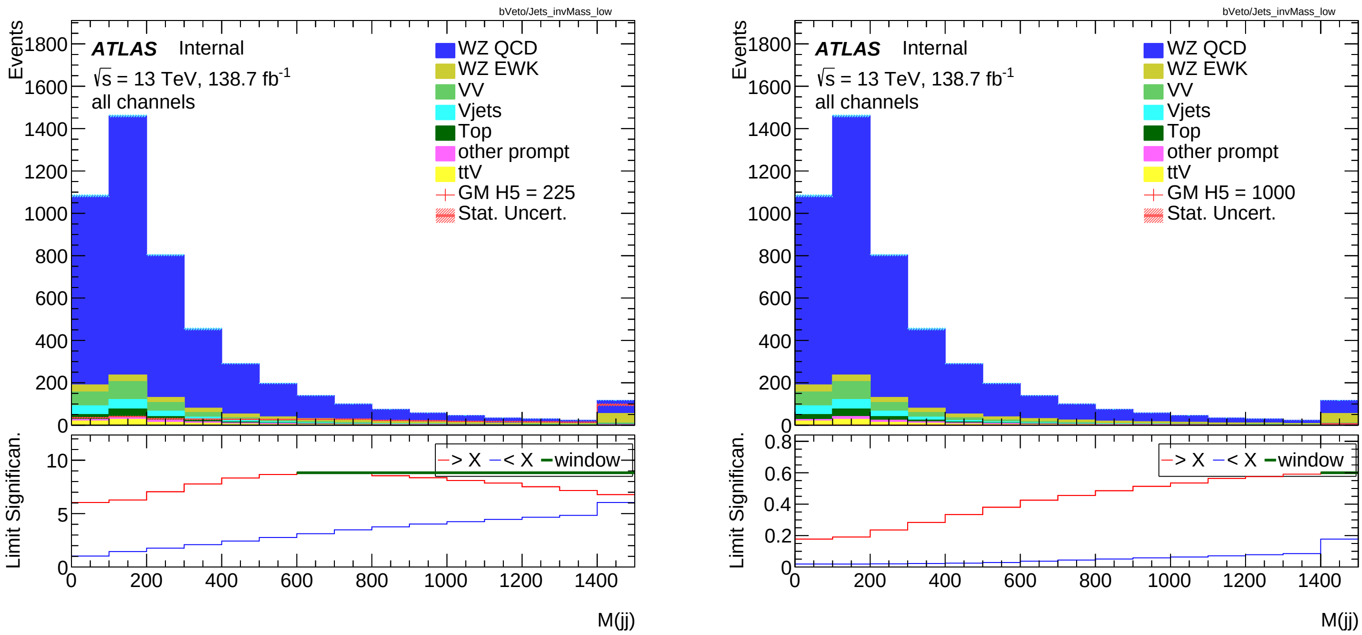

Abb. B.1.: Distribution of event yields for invariant mass after bVeto selection, including limit significance subplot, for lowest GM225 (left) and highest masspoint GM1000 (right)

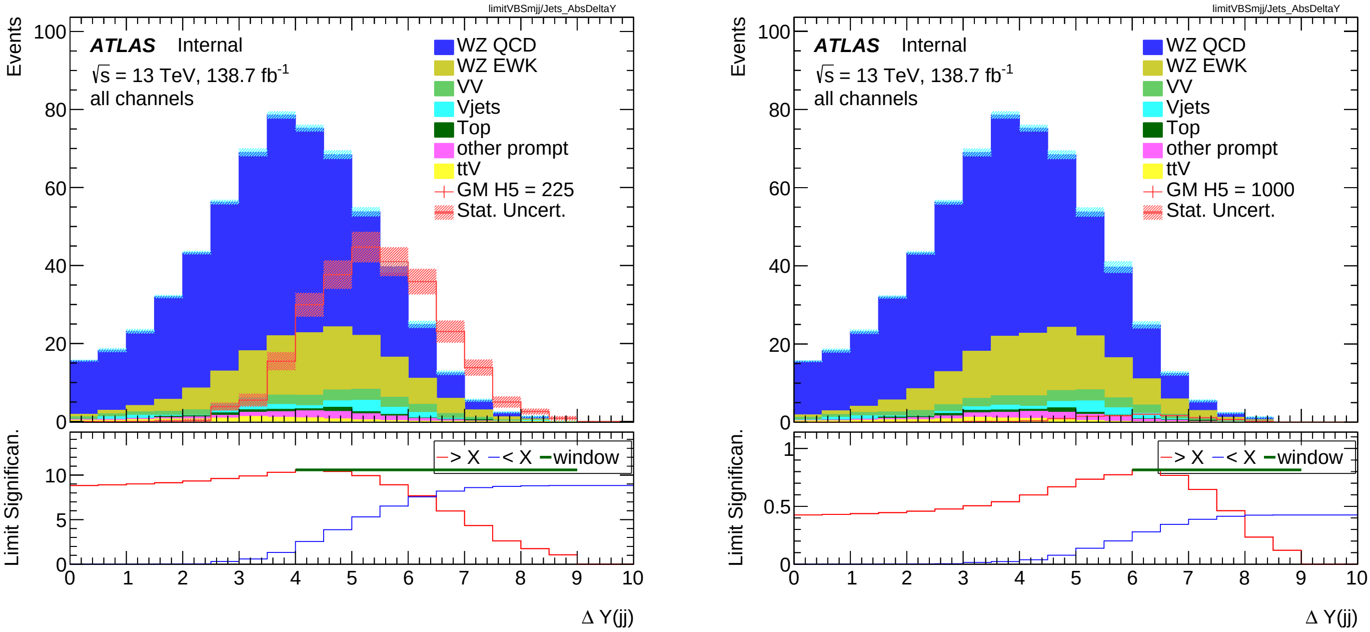

Abb. B.2.: Distribution of event yields for rapidity difference of the tagging jets after new m_{jj} selection, including limit significance subplot, for lowest GM225 (left) and highest masspoint GM1000 (right)

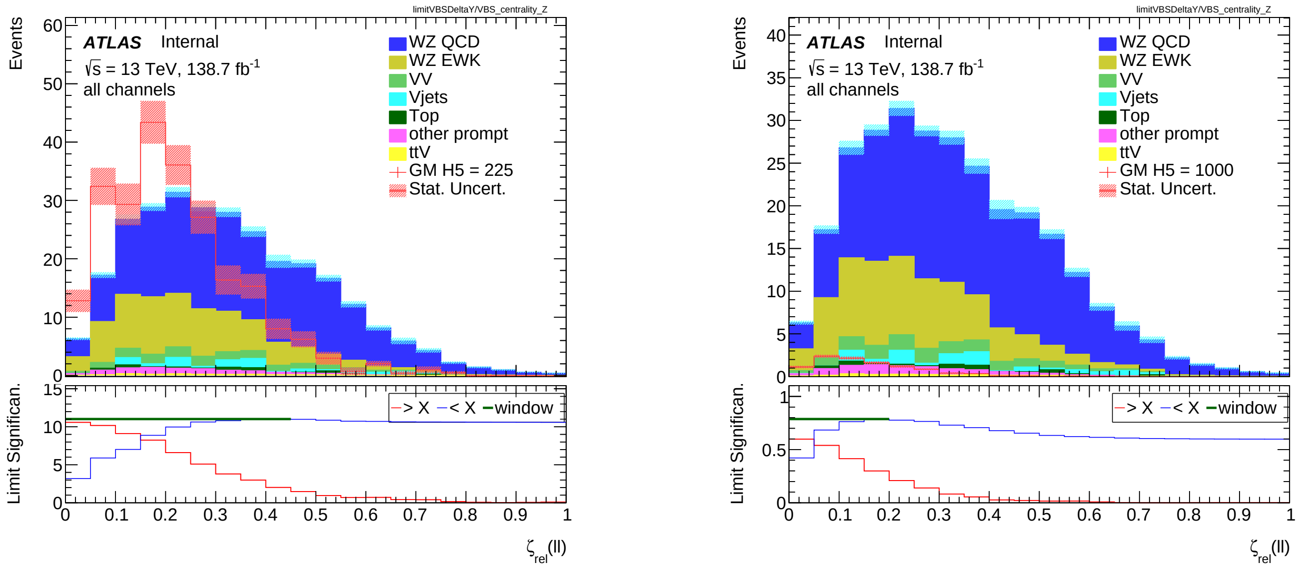

Abb. B.3.: Distribution of event yields for Z centrality after new ΔY_{jj} selection, including limit significance subplot, for lowest GM225 (left) and highest masspoint GM1000 (right)

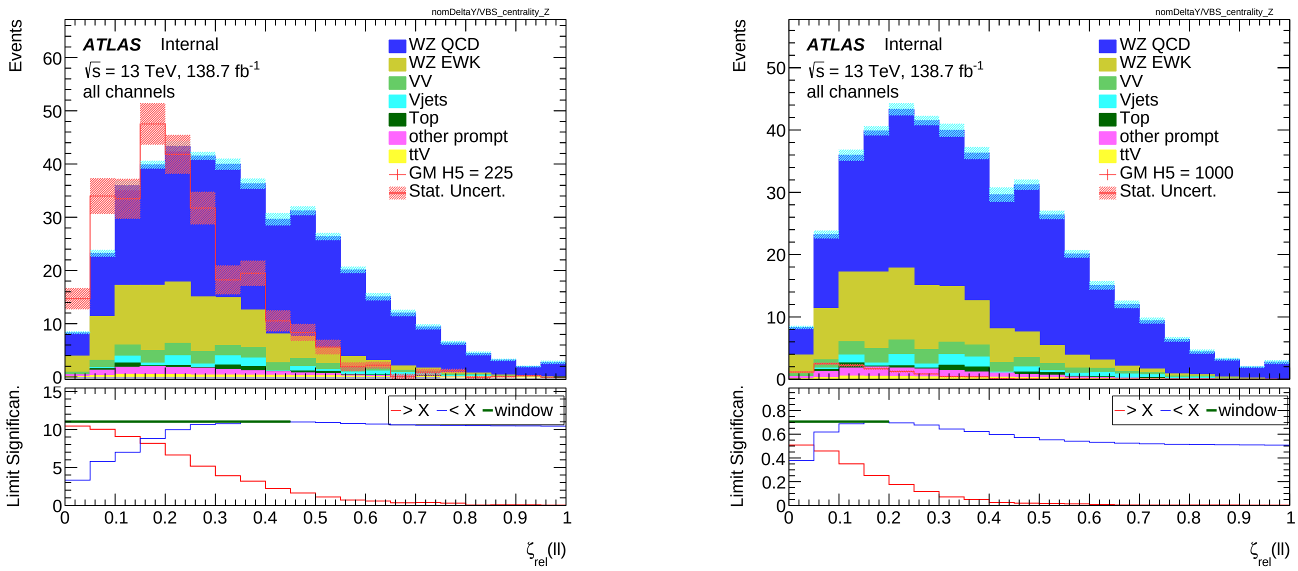

Abb. B.4.: Distribution of event yields for Z centrality after nominal m_{jj} and ΔY_{jj} selection, including limit significance subplot, for lowest GM225 (left) and highest masspoint GM1000 (right)

C. Tables - with event numbers and figures of merit

C.1. nominal selection

GM225	bVeto		m_{jj} > 500		ΔY_{jj} > 3.5	
WZ QCD	3997.4640	± 9.1609	594.5188	± 2.7582	287.1629	± 2.4133
WZ EWK	259.1018	± 0.6979	132.5242	± 0.5098	90.7686	± 0.4230
VV	261.6673	± 1.2497	34.7817	± 0.4675	21.7771	± 0.4451
Vjets	152.2195	± 7.0084	19.6416	± 2.7094	11.8692	± 1.6778
Top	95.5719	± 3.6305	7.9304	± 1.0467	4.5177	± 0.7799
other prompt	58.4022	± 0.2654	16.2365	± 0.1290	10.9348	± 0.1031
ttV	83.6490	± 0.6823	11.1061	± 0.2615	4.0047	± 0.1454
GM H5 = 225	447.4782	± 12.2090	286.7380	± 9.8048	271.8451	± 9.4943
total BKG	4908.0756	± 12.1986	816.7393	± 4.0752	431.0350	± 3.1074
FoM_1	6.1146 ± 0.1600		8.6318 ± 0.2573		10.2537 ± 0.2898	
FoM_2	0.2880 ± 0.0083		1.1011 ± 0.0400		1.9577 ± 0.0728	

Tab. C.1.: Event yields for background and 225 GeV masspoint contributions with calculated figures of merit of current selection

GM1000	bVeto		m_{jj} > 500		ΔY_{jj} > 3.5	
WZ QCD	3997.4640	± 9.1609	594.5188	± 2.7582	287.1629	± 2.4133
WZ EWK	259.1018	± 0.6979	132.5242	± 0.5098	90.7686	± 0.4230
VV	261.6673	± 1.2497	34.7817	± 0.4675	21.7771	± 0.4451
Vjets	152.2195	± 7.0084	19.6416	± 2.7094	11.8692	± 1.6778
Top	95.5719	± 3.6305	7.9304	± 1.0467	4.5177	± 0.7799
other prompt	58.4022	± 0.2654	16.2365	± 0.1290	10.9348	± 0.1031
ttV	83.6490	± 0.6823	11.1061	± 0.2615	4.0047	± 0.1454
GM H5 = 1000	12.6374	± 0.4424	11.0315	± 0.4084	10.7562	± 0.4025
total BKG	4908.0756	± 12.1986	816.7393	± 4.0752	431.0350	± 3.1074
FoM_1	0.1802 ± 0.0063		0.3834 ± 0.0141		0.5117 ± 0.0190	
FoM_2	0.0083 ± 0.0003		0.0424 ± 0.0017		0.0780 ± 0.0031	

Tab. C.2.: Event yields for background and 1000 GeV masspoint contributions with calculated figures of merit of current selection

C.2. nominal + centrality selection:

GM225	bVeto		m_{jj} > 500		ΔY_{jj} > 3.5		$\zeta(Z)$ < 0.4	
WZ QCD	3997.4640	± 9.1609	594.5188	± 2.7582	287.1629	± 2.4133	158.4599	± 1.6379
WZ EWK	259.1018	± 0.6979	132.5242	± 0.5098	90.7686	± 0.4230	72.5732	± 0.3786
VV	261.6673	± 1.2497	34.7817	± 0.4675	21.7771	± 0.4451	14.8607	± 0.3172
Vjets	152.2195	± 7.0084	19.6416	± 2.7094	11.8692	± 1.6778	7.8074	± 1.3885
Top	95.5719	± 3.6305	7.9304	± 1.0467	4.5177	± 0.7799	3.3431	± 0.6766
other prompt	58.4022	± 0.2654	16.2365	± 0.1290	10.9348	± 0.1031	8.6561	± 0.0906
ttV	83.6490	± 0.6823	11.1061	± 0.2615	4.0047	± 0.1454	2.7922	± 0.1212
GM H5 = 225	447.4782	± 12.2090	286.7380	± 9.8048	271.8451	± 9.4943	240.9394	± 8.9378
total BKG	4908.0756	± 12.1986	816.7393	± 4.0752	431.0350	± 3.1074	268.4926	± 2.3098
FoM_1	6.1146 ± 0.1600		8.6318 ± 0.2573		10.2537 ± 0.2898		10.6749 ± 0.3033	
FoM_2	0.2880 ± 0.0083		1.1011 ± 0.0400		1.9577 ± 0.0728		2.7425 ± 0.1076	

Tab. C.3.: Event yields for background and 225 GeV masspoint contributions with calculated figures of merit of current selection with additional centrality selection, centrality cut value determined by significance subplot

GM1000	bVeto		m_{jj} > 500		ΔY_{jj} > 3.5		$\zeta(Z)$ < 0.4	
WZ QCD	3997.4640	± 9.1609	594.5188	± 2.7582	287.1629	± 2.4133	158.4599	± 1.6379
WZ EWK	259.1018	± 0.6979	132.5242	± 0.5098	90.7686	± 0.4230	72.5732	± 0.3786
VV	261.6673	± 1.2497	34.7817	± 0.4675	21.7771	± 0.4451	14.8607	± 0.3172
Vjets	152.2195	± 7.0084	19.6416	± 2.7094	11.8692	± 1.6778	7.8074	± 1.3885
Top	95.5719	± 3.6305	7.9304	± 1.0467	4.5177	± 0.7799	3.3431	± 0.6766
other prompt	58.4022	± 0.2654	16.2365	± 0.1290	10.9348	± 0.1031	8.6561	± 0.0906
ttV	83.6490	± 0.6823	11.1061	± 0.2615	4.0047	± 0.1454	2.7922	± 0.1212
GM H5 = 1000	12.6374	± 0.4424	11.0315	± 0.4084	10.7562	± 0.4025	10.4361	± 0.3906
total BKG	4908.0756	± 12.1986	816.7393	± 4.0752	431.0350	± 3.1074	268.4926	± 2.3098
FoM_1	0.1802 ± 0.0063		0.3834 ± 0.0141		0.5117 ± 0.0190		0.6249 ± 0.0231	
FoM_2	0.0083 ± 0.0003		0.0424 ± 0.0017		0.0780 ± 0.0031		0.1206 ± 0.0049	

Tab. C.4.: Event yields for background and 1000 GeV masspoint contributions with calculated figures of merit of current selection with additional centrality selection, centrality cut value determined by significance subplot

C.3. new selection:

GM 225	bVeto		m_{jj} > 700		ΔY_{jj} > 4.5		$\zeta(Z)$ < 0.4		81.1876 < $M(Z)$ < 101.1876	
WZ QCD	3997.4640	± 9.1609	327.2630	± 2.0450	105.1764	± 1.7656	69.2643	± 1.1755	64.9438	± 1.1379
WZ EWK	259.1018	± 0.6979	103.9563	± 0.4548	51.6654	± 0.3220	44.5465	± 0.2992	41.7865	± 0.2897
VV	261.6673	± 1.2497	20.0518	± 0.3006	10.4484	± 0.2725	8.0064	± 0.2431	7.4528	± 0.2364
Vjets	152.2195	± 7.0084	10.0121	± 1.5300	6.7862	± 1.3141	4.6737	± 1.0855	3.2399	± 0.8833
Top	95.5719	± 3.6305	3.5950	± 0.6996	2.0426	± 0.5163	1.8011	± 0.4891	1.0385	± 0.3753
other prompt	58.4022	± 0.2654	9.7848	± 0.0991	5.3061	± 0.0717	4.5720	± 0.0657	4.3032	± 0.0633
ttV	83.6490	± 0.6823	5.7763	± 0.1889	1.3487	± 0.0827	1.0620	± 0.0735	0.9626	± 0.0703
GM H5 = 225	447.4782	± 12.2090	231.9221	± 8.8094	191.9736	± 8.0155	180.3420	± 7.6976	172.4798	± 7.5022
total BKG	4908.0756	± 12.1986	480.4394	± 2.7120	182.7738	± 2.3024	133.9259	± 1.7198	123.7274	± 1.5377
FoM_1	6.1146 ± 0.1600		8.6894 ± 0.2768		9.9168 ± 0.3100		10.1729 ± 0.3109		10.0217 ± 0.3101	
FoM_2	0.2880 ± 0.0083		1.5035 ± 0.0604		3.1495 ± 0.1392		3.9280 ± 0.1733		4.0352 ± 0.1797	

Tab. C.5.: Event yields for background and 225 GeV masspoint contributions with calculated figures of merit for new selection with typical VBS variables, cut values determined by significance subplot

GM 1000	bVeto		mjj > 700		ΔY_{jj} > 4.5		$\zeta(Z)$ < 0.4		81.1876 < $M(Z)$ < 101.1876	
WZ QCD	3997.4640	± 9.1609	327.2630	± 2.0450	105.1764	± 1.7656	69.2643	± 1.1755	64.9438	± 1.1379
WZ EWK	259.1018	± 0.6979	103.9563	± 0.4548	51.6654	± 0.3220	44.5465	± 0.2992	41.7865	± 0.2897
VV	261.6673	± 1.2497	20.0518	± 0.3006	10.4484	± 0.2725	8.0064	± 0.2431	7.4528	± 0.2364
Vjets	152.2195	± 7.0084	10.0121	± 1.5300	6.7862	± 1.3141	4.6737	± 1.0855	3.2399	± 0.8833
Top	95.5719	± 3.6305	3.5950	± 0.6996	2.0426	± 0.5163	1.8011	± 0.4891	1.0385	± 0.3753
other prompt	58.4022	± 0.2654	9.7848	± 0.0991	5.3061	± 0.0717	4.5720	± 0.0657	4.3032	± 0.0633
ttV	83.6490	± 0.6823	5.7763	± 0.1889	1.3487	± 0.0827	1.0620	± 0.0735	0.9626	± 0.0703
GM H5 = 1000	12.6374	± 0.4424	10.1355	± 0.3889	9.5973	± 0.3695	9.4442	± 0.3622	8.7035	± 0.3495
total BKG	4908.0756	± 12.1986	480.4394	± 2.7120	182.7738	± 2.3024	133.9259	± 1.7198	123.7274	± 1.5377
FoM_1	0.1802 ± 0.0063		0.4576 ± 0.0174		0.6920 ± 0.0263		0.7887 ± 0.0296		0.7563 ± 0.0297	
FoM_2	0.0081 ± 0.0003		0.0660 ± 0.0027		0.1615 ± 0.0068		0.2145 ± 0.0091		0.2134 ± 0.0094	

Tab. C.6.: Event yields for background and 1000 GeV masspoint contributions with calculated figures of merit for new selection with typical VBS variables, cut values determined by significance subplot

C.4. high mass signal region:

GM475	$\zeta(Z) < 0.4$		$p_T(Z)/M(WZ) > 0.3$		$p_T(W)/M(WZ) > 0.25$		$L_T > 250$ GeV		$\Delta\Phi(l_W, E_T^{miss}) < 1.2$	
WZ QCD	69.2643	± 1.1755	34.4711	± 0.7708	23.9750	± 0.6582	11.3259	± 0.4400	7.8146	± 0.3520
WZ EWK	44.5465	± 0.2992	22.6085	± 0.2141	14.7495	± 0.1732	8.2741	± 0.1305	6.1371	± 0.1127
VV	8.0064	± 0.2431	3.1007	± 0.1714	1.7701	± 0.1548	0.5452	± 0.0619	0.3499	± 0.0565
Vjets	4.6737	± 1.0855	3.1834	± 0.9094	1.2065	± 0.5267	0.0313	± 0.0157	0.0166	± 0.0117
Top	1.8011	± 0.4891	0.4286	± 0.2485	0.2760	± 0.1962	0.1519	± 0.1519	0.1519	± 0.1519
VVV	0.2734	± 0.0228	0.1267	± 0.0136	0.1039	± 0.0123	0.0619	± 0.0089	0.0411	± 0.0070
ttV	1.0620	± 0.0735	0.7033	± 0.0605	0.5295	± 0.0519	0.2971	± 0.0388	0.2459	± 0.0350
GM H5 = 475	146.2869	± 10.1546	131.5941	± 9.3666	122.7543	± 9.0583	108.3759	± 8.5987	92.3764	± 7.9983
total BKG	129.6274	± 1.7187	64.6223	± 1.2498	42.6106	± 0.8977	20.6874	± 0.4892	14.7571	± 0.4053
FoM_1	8.8068 ± 0.4501		9.3944 ± 0.4455		9.5459 ± 0.4437		9.5396 ± 0.4395		8.9248 ± 0.4400	
FoM_2	3.3075 ± 0.2339		5.3115 ± 0.3548		6.5904 ± 0.4141		8.2669 ± 0.4531		8.1361 ± 0.4541	

Tab. C.7.: Event yields for background and 475 GeV masspoint contributions with calculated figures of merit for high mass signal region selection with new variables, cut values determined by significance subplot

GM1000	$\zeta(Z) < 0.4$		$p_T(Z)/M(WZ) > 0.3$		$p_T(W)/M(WZ) > 0.25$		$L_T > 250$ GeV		$\Delta\Phi(l_W, E_T^{miss}) < 1.2$	
WZ QCD	69.2643	± 1.1755	34.4711	± 0.7708	23.9750	± 0.6582	11.3259	± 0.4400	7.8146	± 0.3520
WZ EWK	44.5465	± 0.2992	22.6085	± 0.2141	14.7495	± 0.1732	8.2741	± 0.1305	6.1371	± 0.1127
VV	8.0064	± 0.2431	3.1007	± 0.1714	1.7701	± 0.1548	0.5452	± 0.0619	0.3499	± 0.0565
Vjets	4.6737	± 1.0855	3.1834	± 0.9094	1.2065	± 0.5267	0.0313	± 0.0157	0.0166	± 0.0117
Top	1.8011	± 0.4891	0.4286	± 0.2485	0.2760	± 0.1962	0.1519	± 0.1519	0.1519	± 0.1519
VVV	0.2734	± 0.0228	0.1267	± 0.0136	0.1039	± 0.0123	0.0619	± 0.0089	0.0411	± 0.0070
ttV	1.0620	± 0.0735	0.7033	± 0.0605	0.5295	± 0.0519	0.2971	± 0.0388	0.2459	± 0.0350
GM H5 = 1000	9.4442	± 0.3622	8.5695	± 0.3428	8.3400	± 0.3394	8.3400	± 0.3394	7.8561	± 0.3294
total BKG	129.6274	± 1.7187	64.6223	± 1.2498	42.6106	± 0.8977	20.6874	± 0.4892	14.7571	± 0.4053
FoM_1	0.8008 ± 0.0301		1.0017 ± 0.0387		1.1684 ± 0.0449		1.5480 ± 0.0555		1.6521 ± 0.0591	
FoM_2	0.2214 ± 0.0094		0.3868 ± 0.0176		0.5469 ± 0.0250		0.9841 ± 0.0425		1.1791 ± 0.0506	

Tab. C.8.: Event yields for background and 1000 GeV masspoint contributions with calculated figures of merit for high mass signal region selection with new variables, cut values determined by significance subplot

C.5. low mass signal region:

GM225	$\zeta(Z) < 0.4$		$p_T(Z)/M(WZ) < 0.3$		$p_T(W)/M(WZ) < 0.25$		$L_T < 250$ GeV		$\Delta\Phi(l_W, E_T^{miss}) > 1.2$	
WZ QCD	69.2643	± 1.1755	34.7931	± 0.8875	13.0252	± 0.6173	12.5218	± 0.6048	12.0587	± 0.5967
WZ EWK	44.5465	± 0.2992	21.9380	± 0.2090	8.4027	± 0.1288	7.3903	± 0.1203	6.7092	± 0.1145
VV	8.0064	± 0.2431	4.9057	± 0.1724	2.1253	± 0.1111	1.9779	± 0.1079	1.8061	± 0.1030
Vjets	4.6737	± 1.0855	1.4903	± 0.5927	0.7865	± 0.4412	0.7747	± 0.4410	0.7633	± 0.4409
Top	1.8011	± 0.4891	1.3725	± 0.4213	0.8148	± 0.3156	0.5960	± 0.2750	0.5960	± 0.2750
VVV	0.2734	± 0.0228	0.1468	± 0.0184	0.0693	± 0.0130	0.0439	± 0.0101	0.0436	± 0.0101
ttV	1.0620	± 0.0735	0.3586	± 0.0418	0.1112	± 0.0230	0.0876	± 0.0210	0.0784	± 0.0204
GM H5 = 225	180.3420	± 7.6976	81.9996	± 5.1376	15.4258	± 2.1336	15.4712	± 2.1253	14.8702	± 2.0902
total BKG	129.6274	± 1.7187	65.0051	± 1.1798	25.3350	± 0.8396	23.3922	± 0.8140	22.0553	± 0.8064
FoM_1	10.2432 ± 0.3113		6.7631 ± 0.3068		2.4162 ± 0.2721		2.4817 ± 0.2743		2.4471 ± 0.2760	
FoM_2	4.0424 ± 0.1781		3.4359 ± 0.2125		1.5058 ± 0.2015		1.5993 ± 0.2103		1.6075 ± 0.2152	

Tab. C.9.: Event yields for background and 225 GeV masspoint contributions with calculated figures of merit for low mass signal region selection with new variables, cut values determined by significance subplot

GM425	$\zeta(Z) < 0.4$		$p_T(Z)/M(WZ) < 0.3$		$p_T(W)/M(WZ) < 0.25$		$L_T < 250$ GeV		$\Delta\Phi(l_W, E_T^{miss}) > 1.2$	
WZ QCD	69.2643	± 1.1755	34.7931	± 0.8875	13.0252	± 0.6173	12.5218	± 0.6048	12.0587	± 0.5967
WZ EWK	44.5465	± 0.2992	21.9380	± 0.2090	8.4027	± 0.1288	7.3903	± 0.1203	6.7092	± 0.1145
VV	8.0064	± 0.2431	4.9057	± 0.1724	2.1253	± 0.1111	1.9779	± 0.1079	1.8061	± 0.1030
Vjets	4.6737	± 1.0855	1.4903	± 0.5927	0.7865	± 0.4412	0.7747	± 0.4410	0.7633	± 0.4409
Top	1.8011	± 0.4891	1.3725	± 0.4213	0.8148	± 0.3156	0.5960	± 0.2750	0.5960	± 0.2750
VVV	0.2734	± 0.0228	0.1468	± 0.0184	0.0693	± 0.0130	0.0439	± 0.0101	0.0436	± 0.0101
ttV	1.0620	± 0.0735	0.3586	± 0.0418	0.1112	± 0.0230	0.0876	± 0.0210	0.0784	± 0.0204
GM H5 = 425	169.5005	± 4.3729	30.0543	± 1.8467	4.3999	± 0.7421	3.9362	± 0.6924	3.2303	± 0.6458
total BKG	129.6274	± 1.7187	65.0051	± 1.1798	25.3350	± 0.8396	23.3922	± 0.8140	22.0553	± 0.8064
FoM_1	9.8004 ± 0.1834		3.0825 ± 0.1606		0.8069 ± 0.1265		0.7530 ± 0.1234		0.6424 ± 0.1207	
FoM_2	3.8098 ± 0.1082		1.3210 ± 0.0849		0.4540 ± 0.0783		0.4346 ± 0.0781		0.3757 ± 0.0767	

Tab. C.10.: Event yields for background and 425 GeV masspoint contributions with calculated figures of merit for low mass signal region selection with new variables, cut values determined by significance subplot

C.6. limit significance - nominal + centrality selection:

GM225	bVeto		m_{jj} > 500		ΔY_{jj} > 3.5		$\zeta(Z)$ < 0.45	
WZ QCD	3997.4640	± 9.1609	594.5188	± 2.7582	287.1629	± 2.4133	179.9977	± 1.9980
WZ EWK	259.1018	± 0.6979	132.5242	± 0.5098	90.7686	± 0.4230	77.9937	± 0.3924
VV	261.6673	± 1.2497	34.7817	± 0.4675	21.7771	± 0.4451	16.4075	± 0.3404
Vjets	152.2195	± 7.0084	19.6416	± 2.7094	11.8692	± 1.6778	7.9401	± 1.3906
Top	95.5719	± 3.6305	7.9304	± 1.0467	4.5177	± 0.7799	3.3507	± 0.6767
other prompt	58.4022	± 0.2654	16.2365	± 0.1290	10.9348	± 0.1031	9.3298	± 0.0947
ttV	83.6490	± 0.6823	11.1061	± 0.2615	4.0047	± 0.1454	3.1011	± 0.1273
GM H5 = 225	447.4782	± 12.2090	286.7380	± 9.8048	271.8451	± 9.4943	251.4758	± 9.1539
total BKG	4908.0756	± 12.1986	816.7393	± 4.0752	431.0350	± 3.1074	298.1205	± 2.5843
FoM_1	6.1146 ± 0.1600		8.6318 ± 0.2573		10.2537 ± 0.2898		10.7269 ± 0.3022	
FoM_2	0.2880 ± 0.0083		1.1011 ± 0.0400		1.9577 ± 0.0728		2.5887 ± 0.1001	

Tab. C.11.: Event yields for background and 225 GeV masspoint contributions with calculated figures of merit of current selection with additional centrality selection, centrality cut value determined by limit significance subplot

GM1000	bVeto		m_{jj} > 500		ΔY_{jj} > 3.5		$\zeta(Z)$ < 0.45	
WZ QCD	3997.4640	± 9.1609	594.5188	± 2.7582	287.1629	± 2.4133	179.9977	± 1.9980
WZ EWK	259.1018	± 0.6979	132.5242	± 0.5098	90.7686	± 0.4230	77.9937	± 0.3924
VV	261.6673	± 1.2497	34.7817	± 0.4675	21.7771	± 0.4451	16.4075	± 0.3404
Vjets	152.2195	± 7.0084	19.6416	± 2.7094	11.8692	± 1.6778	7.9401	± 1.3906
Top	95.5719	± 3.6305	7.9304	± 1.0467	4.5177	± 0.7799	3.3507	± 0.6767
other prompt	58.4022	± 0.2654	16.2365	± 0.1290	10.9348	± 0.1031	9.3298	± 0.0947
ttV	83.6490	± 0.6823	11.1061	± 0.2615	4.0047	± 0.1454	3.1011	± 0.1273
GM H5 = 1000	12.6374	± 0.4424	11.0315	± 0.4084	10.7562	± 0.4025	10.5393	± 0.3940
total BKG	4908.0756	± 12.1986	816.7393	± 4.0752	431.0350	± 3.1074	298.1205	± 2.5843
FoM_1	0.1802 ± 0.0063		0.3834 ± 0.0141		0.5117 ± 0.0190		0.5999 ± 0.0222	
FoM_2	0.0081 ± 0.0003		0.0424 ± 0.0017		0.0780 ± 0.0031		0.1099 ± 0.0044	

Tab. C.12.: Event yields for background and 1000 GeV masspoint contributions with calculated figures of merit of current selection with additional centrality selection, centrality cut value determined by limit significance subplot

C.7. limit significance - new selection:

GM 225	bVeto		m_{jj} > 600		ΔY_{jj} > 4		$\zeta(Z)$ < 0.45	
WZ QCD	3997.4640	± 9.1609	436.5499	± 2.4211	176.3053	± 2.0259	119.8492	± 1.7481
WZ EWK	259.1018	± 0.6979	117.4388	± 0.4817	69.8196	± 0.3726	62.1091	± 0.3516
VV	261.6673	± 1.2497	26.1173	± 0.3457	15.1331	± 0.3191	11.9587	± 0.2922
Vjets	152.2195	± 7.0084	13.8401	± 1.7979	9.1513	± 1.5095	6.6204	± 1.2926
Top	95.5719	± 3.6305	5.4763	± 0.8642	3.0976	± 0.6396	2.3406	± 0.5591
other prompt	58.4022	± 0.2654	12.5811	± 0.1132	7.7302	± 0.0865	6.8152	± 0.0809
ttV	83.6490	± 0.6823	7.8766	± 0.2216	2.3749	± 0.1110	1.8728	± 0.0996
GM H5 = 225	447.4782	± 12.2090	259.6961	± 9.3078	234.4779	± 8.7874	220.7923	± 8.5438
total BKG	4908.0756	± 12.1986	619.8801	± 3.2023	283.6120	± 2.6556	211.5659	± 2.2945
FoM_1	6.1146 ± 0.1600		8.7565 ± 0.2680		10.3015 ± 0.2999		10.6185 ± 0.3073	
FoM_2	0.2880 ± 0.0083		1.3099 ± 0.0497		2.5341 ± 0.1011		3.1515 ± 0.1291	

Tab. C.13.: Event yields for background and 225 GeV masspoint contributions with calculated figures of merit of new selection with typical VBS variables, cut values determined by limit significance subplot

GM 1000	bVeto		mjj > 600		ΔY_{jj} > 4		$\zeta(Z)$ < 0.45	
WZ QCD	3997.4640	± 9.1609	436.5499	± 2.4211	176.3053	± 2.0259	119.8492	± 1.7481
WZ EWK	259.1018	± 0.6979	117.4388	± 0.4817	69.8196	± 0.3726	62.1091	± 0.3516
VV	261.6673	± 1.2497	26.1173	± 0.3457	15.1331	± 0.3191	11.9587	± 0.2922
Vjets	152.2195	± 7.0084	13.8401	± 1.7979	9.1513	± 1.5095	6.6204	± 1.2926
Top	95.5719	± 3.6305	5.4763	± 0.8642	3.0976	± 0.6396	2.3406	± 0.5591
other prompt	58.4022	± 0.2654	12.5811	± 0.1132	7.7302	± 0.0865	6.8152	± 0.0809
ttV	83.6490	± 0.6823	7.8766	± 0.2216	2.3749	± 0.1110	1.8728	± 0.0996
GM H5 = 1000	12.6374	± 0.4424	10.7398	± 0.3989	10.3200	± 0.3887	10.1307	± 0.3820
total BKG	4908.0756	± 12.1986	619.8801	± 3.2023	283.6120	± 2.6556	211.5659	± 2.2945
FoM_1	0.1802 ± 0.0063		0.4277 ± 0.0158		0.6019 ± 0.0224		0.6804 ± 0.0253	
FoM_2	0.0081 ± 0.0003		0.0543 ± 0.0021		0.1130 ± 0.0046		0.1478 ± 0.0061	

Tab. C.14.: Event yields for background and 1000 GeV masspoint contributions with calculated figures of merit of new selection with typical VBS variables, cut values determined by limit significance subplot

D. Background process

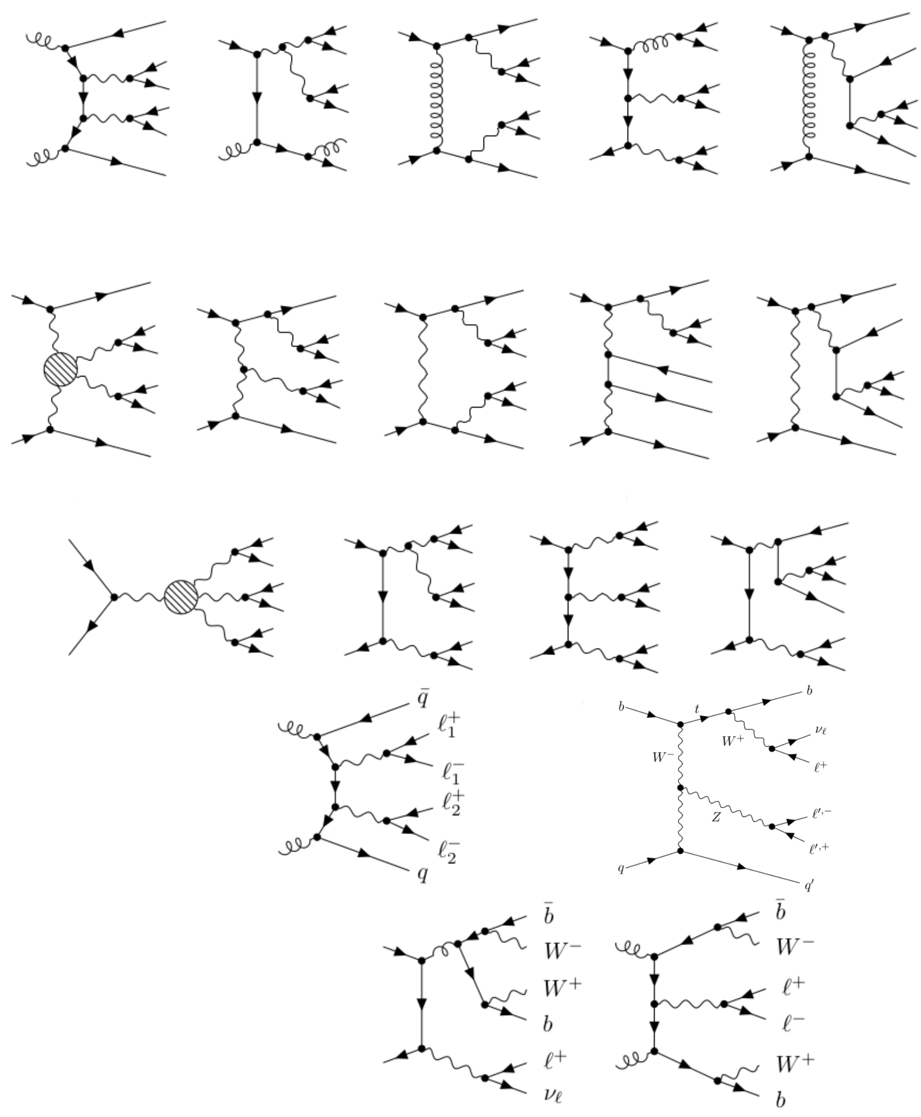

Abb. D.1.: Examples for background process in the considered lvvl final state, the hatched circled replaces all possible processes for SM VBS
first row: WZ QCD; second/third row: WZ EWK; fourth row: ZZ (left) and tZj (right); fifth row: ttV
straight line represents fermion; wiggly line represents electroweak boson, helix line represents gluon [2]

E. Preselection

	Selection	Motivation
lepton selection	Single lepton trigger	High efficiency 3 leptons
	High p_T leptons (>25GeV)	
	must come from primary vertex, cuts on impact parameters	Reduce background from QCD, Z+jet, tt and single top
	Calorimeter and track isolation	
	Only 3 good lepton (additional 20 GeV leptons)	Reduce ZZ background
Z selection	Pair of same flavor, opposite sign	Reduce non peaking background like tt and single top
	consistent with Z boson in a ±20 GeV window around invariant Z mass	
	if more than one pair, select the closest to Z mass	
W Selection	Additional "tight"lepton requirement	Reduce the Z+jets and top background
	$E_T^{miss} > 25GeV$	To account for W and reduce Z+jets

Tab. E.1.: List of preselection requirements for data measurements at the ATLAS detector [13]

Literatur

1. THOMSON, M.: Modern Particle Physics. In: 6. Aufl. Cambridge: Cambridge University Press, 2013, cit. on p. 3, 6, 8.
2. BITTRICH, C.: *Evidence for Scattering of Electroweak Gauge Bosons in the $W \pm Z$ Channel with the ATLAS Detector at the Large Hadron Collider.* 2020. Diss. Technische Universität Dresden, cit. on p. 20, 23-26, 96.
3. AL., G. A. et: Search for resonant W±Z $\longrightarrow \ell\nu\ell\ell$ Production in Run-2 $\sqrt{}$ of the LHC Proton-Proton Collisions at s = 13TeV with ATLAS Detector. 2020, cit. on p. 7.
4. COLLABORATION, A.: The ATLAS Experiment at the CERN Large Hadron Collider. *JINST 3 S08003.* 2008, cit. on p. 4.
5. PEREZ, G.: *Unitarization Models For Vector Boson Scattering at the LHC.* 2018. Abger. unter DOI: 10.5445/IR/1000082199,cit.onp.23. Diss.
6. REYGERS, P. D. K.: *Quark-Gluon Plasma Physics.* 2020-06-16, cit. on p. 11. Auch verfügbar unter: https://www.physi.uni-heidelberg.de/~reygers/lectures/2017/qgp/qgp_ss17_02_kinematics.pdf.
7. K. KRÖNINGER, e. a.: *Data Analysis in High Energy Physics.* Weinheim, Germany: WILEY-VCH Verlag GmbH Co. KGaA, 2013, cit. on p. 83-85.
8. COWAN, G.: *Statistics.* 2017, cit. on p. 37-40. Auch verfügbar unter: https://pdg.lbl.gov/2018/reviews/rpp2018-rev-statistics.pdf.
9. RAMOS, J. M.: *2021 Hands-on Particle Physics.* [o.D.].
10. NAG, A.; RAMOS, J. M.: *WZ Resonance search Status Update.* cit. on p. 17. Auch verfügbar unter: file:///home/iktp/Documents/WZ_Resonance_Status.pdf.
11. GASIOROWSKI, S.: *Upper Limit Calculation.* cit. on p. 3,5. Auch verfügbar unter: https://indico.cern.ch/event/562534/contributions/2272566/attachments/1322215/1983432/Upper_Limit_Presentation.pdf.
12. COLLABORATION, A.: Measurements of WZ production cross sections in pp collisions at ffiffi s p = 8 TeV with the ATLAS detector and limits on anomalous gauge boson self-couplings. 13 May 2016. Auch verfügbar unter: https://journals.aps.org/prd/pdf/10.1103/PhysRevD.93.092004.
13. RAMOS, J. M.: *Search for resonant WZ Production with the ATLAS detector at the LHC.* March 21, 2018, cit. on p. 7.

Selbstständigkeitserklärung

Hiermit erkläre ich, dass ich diese Arbeit im Rahmen der Betreuung am *Institut für Kern- und Teilchephysik* ohne unzulässige Hilfe Dritter verfasst und alle Quellen als solche gekennzeichnet habe.

Dennis Kraft,
Berlin, 6. Juli 2021